

Jet directions in Seyfert galaxies: B and I imaging data

H. R. Schmitt^{1,2,3,4,6}, A. L. Kinney^{1,2,3,5}

ABSTRACT

We present the results of broad-band B and I imaging observations for a sample of 88 Seyfert galaxies (29 Seyfert 1's and 59 Seyfert 2's), selected from a mostly isotropic property, the flux at $60\mu\text{m}$. We also present the B and I imaging results for an additional sample of 20 Seyfert galaxies (7 Seyfert 1's and 13 Seyfert 2's), selected from the literature and known to have extended radio emission. The I band images are fitted with ellipses to determine the position angle and ellipticity of the host galaxy major axis. This information will be used in a future paper, combined with information from radio observations, to study the orientation of radio jets relative to the plane of their host galaxies (Kinney et al. 2000). Here we present surface brightness profiles and magnitudes in the B and I bands, as well as mean ellipticities and major axis position angles.

Subject headings: galaxies:active – galaxies:structure – galaxies:Seyfert – galaxies:photometry

1. Introduction

We have recently shown (Schmitt et al. 1997; Clarke, Kinney & Pringle 1998; see also Nagar & Wilson 1999) that there is no correlation between the position angle of radio jets and disk major axes in Seyfert galaxies, confirming previous results based on smaller samples (Ulvestad & Wilson 1984; Brindle et al. 1990; Baum et al. 1993). Clarke et al. (1998) and Nagar & Wilson (1999) showed, using a statistical inversion technique, that the observed values of δ (the difference between the position angle of the jet and the host galaxy disk major axis) and i (inclination of

¹Space Telescope Science Institute, 3700 San Martin Drive, Baltimore, MD 21218, USA

²Visiting Astronomer Cerro Tololo Interamerican Observatory, National Optical Astronomy Observatories, which is operated by AURA, Inc. under a cooperative agreement with the National Science Foundation

³Visiting Astronomer Kitt Peak National Observatory National Optical Astronomy Observatories, which is operated by AURA, Inc. under a cooperative agreement with the National Science Foundation

⁴Visiting Astronomer Lick Observatory, operated by the University of California Observatories

⁵Present address: NASA Headquarters, 300 E St., Washington, DC20546

⁶email:schmitt@stsci.edu

the galaxy disk relative to the line of sight) can be reproduced by a homogeneous distribution of angles β between the jet and the galaxy disk axis.

These results contradict the expectation that the jets should be aligned perpendicular to the galaxy disk. The simplest assumption about the feeding of the accretion disk and the black hole suggests that the gas comes from the host galaxy disk, so it is natural to expect both disks to be aligned and have the same angular momentum vector. Since jets are emitted perpendicular to the accretion disk, we would expect them to be aligned with the host galaxy minor axis, which is not observed. These studies give us information about the inner workings of Seyferts and may shed some light on the processes involved in the feeding of the AGN.

Although the results from Clarke et al. (1998) and Nagar & Wilson (1999) were statistically significant, they had two major limitations, their samples and most of their measurements were obtained from the literature. This indicates that their results could be biased by selection effects, like the preferential selection of galaxies which have jets shining into the plane of the galaxy, resulting in brighter radio emission and narrow line regions, which would be easier to detect. From the point of view of the data, using measurements collected from the literature can also influence the results, since different authors are likely to measure the position angle of radio jets, the disk inclination and the position angle of the host galaxy major axis using different techniques and data of different quality.

In order to improve the data relative to previous studies, we obtained radio continuum maps at 3.6cm, optical broad band images and spectroscopy for a sample of Seyfert galaxies selected from a mostly isotropic property, the flux at $60\mu\text{m}$. In this way we avoid selection effects and create a homogeneous database, with measurements done using a consistent technique.

Another possible improvement which will be used in the analysis paper (Kinney et al. 2000), is the distinction between which side of the galaxy minor axis is closer to Earth. According to Clarke et al. (1998), this information can improve the statistical determination of the β -distribution by a factor of 2. One way to obtain this information is from the inspection of dust lanes in the galaxies' images. Dust lanes can be seen in the near side of the galaxy, because they are highlighted against the background bulge light. Due to this fact, we decided to obtain images in the B and I bands, with a large wavelength separation, which will allow us to search for dust lanes. Another way to obtain this information is from the rotation curve of the galaxy. Knowing which side of the galaxy is approaching us and assuming that the spiral arms are trailing, we can determine which side of the minor axis is closer to Earth. In order to do this, we obtained long-slit spectra, with the slit aligned close to the host galaxy major axis, for several objects in our sample.

In this paper we present the broad-band B and I imaging data. The radio continuum observations and optical spectroscopic data will be presented elsewhere. In Section 2 we present the samples used in our study. The description of the observations and reductions is given in Section 3, and the measurements are presented in Section 4. A summary is given in Section 5.

2. Sample

2.1. $60\mu\text{m}$ sample

In order to avoid selection effects as much as possible, we have chosen a sample from a mostly isotropic property, the flux at $60\mu\text{m}$. According to the torus models of Pier & Krolik (1992), which are the most anisotropic and hence the most conservative models, the circumnuclear torus radiates nearly isotropically at $60\mu\text{m}$.

Our sample includes 88 Seyfert galaxies (29 Seyfert 1's and 59 Seyfert 2's), which correspond to all galaxies from the de Grijp et al. (1987, 1992) sample of warm IRAS galaxies with redshift $z \leq 0.031$. The galaxies in this sample were selected based on the quality of the $60\mu\text{m}$ flux, Galactic latitude $|b| > 20^\circ$, and $25\mu\text{m} - 60\mu\text{m}$ color in the range $-1.5 < \alpha(25/60) < 0$, chosen to exclude starburst galaxies as much as possible. The candidate AGN galaxies were all observed spectroscopically (de Grijp et al. 1992) to confirm their activity class as being Seyfert 1 or Seyfert 2 and *not* a lower level of activity such as starburst or LINER. The distance limit of $z \leq 0.031$ is large enough to encompass a statistically significant number of objects yet close enough to ensure that radio features can be resolved.

Table 1 presents the galaxies in the de Grijp et al. (1987) catalog, selected for our study. We list their catalog numbers, names, coordinates, the total exposure times in the B and I bands, and the observing runs in which the galaxies were observed.

2.2. Additional sample

Parts of the study presented by Kinney et al. (2000) will also use an additional sample of 53 Seyfert galaxies selected from the literature. This sample comprises Seyferts known to have extended radio emission, used in previous studies (such as Schmitt et al. 1997; or Nagar et al. 1999) but which are not in the $60\mu\text{m}$ sample. For 20 of these galaxies (7 Seyfert 1's and 13 Seyfert 2's) we were able to obtain B and/or I images during our observing runs. Table 2 gives the names of the galaxies, their coordinates, total exposure times in B and I bands and the observing run in which they were observed.

Some of the galaxies in the additional sample were used in previous papers, but we now consider that they should not be included in this analysis. The reasons to exclude them are the fact that they are in interacting systems, mergers, or the radio emission is not extended enough to allow a reliable measurement of the position angle of the jet. For these galaxies, Column 8 (Comments) of Table 2 gives the reasons why they are excluded.

3. Observations and reductions

The data presented in this paper were obtained in 5 different observing runs, using 3 different observatories. The dates of these observing runs, corresponding telescopes and instruments are shown in Table 3.

The CTIO observations were done in the 0.9m telescope with focal ratio $f/13.5$, using the detector T2K6 for run *a* and detector T2K3 for run *d*. Both CCD's have the same plate scale, which gives a pixel size of $0.384''/pixel^{-1}$. The images in run *a* were obtained using the whole CCD area of 2048×2048 pixels, reading it out using 4 different amplifiers, which gives a field of view of $\approx 13' \times 13'$. For run *d* we used only a 1024×1024 section of the CCD, reading it out using one amplifier, which gives a field of view of $\approx 7.5' \times 7.5'$.

The observations at Lick Observatory were done in the 1.0m Nickel telescope with focal ratio $f/17$, using Dewar #5 in both runs (*b* and *c*), which gives a pixel size of $0.248''/pixel^{-1}$. We used the whole CCD area (1024×1024 pixels) for these observations, which gives a field of view of $\approx 4.8' \times 4.8'$. The KPNO observations were done in the 0.9m telescope with focal ratio $f/7.5$, using the detector T2KA, which gives a pixel size of $0.688''/pixel^{-1}$. We used only a 1024×1024 section of the CCD, which gives a field of view of $\approx 11.7' \times 11.7'$.

We followed the same observing procedure for each one of the runs. For each night we obtained a series of bias images (between 20 and 50 exposures), dome flats (between 15 and 30 exposures per filter) and sky flats (between 5 and 10 exposures per filter). We did not obtain dark images, because our exposure times were short enough that the contribution of dark current was negligible.

The reductions were done following standard IRAF procedures. The individual images were overscanned, bias subtracted and divided by the normalized flat field. Tests showed that, for each observing run, there was no significant differences between calibration frames from individual nights. Therefore, all frames were combined and we used the resulting images, which had a higher S/N, for the data reduction. The images were flat-fielded using only the sky flats, since tests showed that the dome flats had inhomogeneous illumination.

To calibrate the images in the Cousins system, each night we observed several standard star fields from Graham (1982) and Landolt (1992). We estimate that the photometric accuracy of our observations is of the order of 0.05 mag. To avoid the saturation of the nuclear region and to eliminate cosmetic defects and cosmic rays, the images were dithered using 3 or more exposures of 400s or less. For three of the galaxies in the $60\mu m$ sample it was possible to obtain images in only one of the bands (I for MRK1040 and B for IRAS16382-0613 and UGC10683B). Furthermore, runs *a* and *e* took place close to full moon, resulting in shallower B images.

Since our images will be used to compare the position angles in the radio and optical, it is important to determine the orientation of the CCD's relative to the equatorial plane. This was done using stars in the images, which showed that the fields are not rotated. The final orientation

of the images is N up and E to the left, with an uncertainty of $\approx 1^\circ$.

4. Measurements

In Figure 1 we present the I band images of the galaxies, organized following the same order of Tables 1 and 2. In the case of UGC10683B and IRAS16382-0613, for which we were not able to obtain I band images, the B band images are shown instead.

Measurements of disk ellipticities and major axis position angles (defined as the angle measured from N to E) were obtained fitting ellipses to the isophotes of the galaxies, using the routine “ellipse” in the STSDAS package of IRAF. We have chosen to fit the ellipses over the I band images because they were deeper, and also because this band is more sensitive to old stars, so the outer isophotes are not disturbed by HII regions like they can be in the B images.

The ellipses were fitted from the inner $\approx 0.7''$ of the I images, out to the level where the surface brightness reached the 3σ level above the background (this limiting value is listed in Tables 4 and 5). The background level and its standard deviation (σ) were determined from several blank regions around the galaxy. For some galaxies, with bright stars close to the low surface brightness isophotes (e.g. NGC3783), the ellipse fitting procedure was truncated before it reached the 3σ level, to avoid the disturbance of the fit by these stars. Ellipses centers were held fixed at the nuclear position, and were fitted using a constant increment of the semi-major axis, 2 pixels for runs *a*, *b*, *c* and *d* and 1 pixel for run *e*, which corresponds to $\approx 0.77''$ for runs *a* and *d*, $\approx 0.5''$ for runs *b* and *c* and $\approx 0.69''$ for run *e*. The surface brightness of the 3σ level in I was typically $21\text{-}22.5 \text{ mag arcsec}^{-2}$, which corresponds to $23\text{-}24.5 \text{ mag arcsec}^{-2}$ in the B band, assuming that the mean color of spiral disks is $(B\text{-}I)\approx 2$ (Héraudeau, Simien & Mamon 1996; see also our own measurements in Figure 2).

The ellipse parameters obtained from the fit of the I band images were used to measure the surface brightness profile of the B images, thus allowing a direct comparison between the two measurements. In Figure 2 we show the surface brightness profiles, major axis position angle (PA_{MA}) and disk ellipticity (e), defined as $e=1-b/a$, where b/a is the ratio between the minor and major axis. Notice that the ellipse parameters in the inner $1'' - 2''$ are unreliable, because they were made on scales smaller or comparable to the seeing.

In Tables 4 and 5, for the $60\mu\text{m}$ and additional samples, respectively, we present the size of the ellipse major axis at the 3σ level above the background, the surface brightness of this level, the integrated magnitude inside this region and the seeing during the observations, for both B and I bands. The integrated magnitudes were calculated by integrating the flux inside the ellipses corresponding to the 3σ isophote, using the major axis lengths given in Tables 4 and 5, the ellipticities and PA_{MA} ’s given in Tables 6 and 7 for the $60\mu\text{m}$ and additional samples, respectively. Notice that, since there is a difference between the 3σ level of the B and I band images, the B images are usually shallower and not as extended as the I images, the ellipse parameters used to

measure the integrated magnitudes of these two bands are slightly different. This is the reason why Tables 6 and 7 give different values of ellipticity and PA_{MA} for B and I bands.

The I band ellipticities and PA_{MA} 's were obtained by averaging the results from the ellipses fitted between the isophotes 3σ and 4σ above the background (4 to 10 points, depending on the galaxy). We adopted this procedure to eliminate large spurious variations, since these values will be combined with radio measurements to study the orientation of radio jets relative to the host galaxy disk axis in these galaxies (Kinney et al. 2000). An inspection of the radial profiles in Figure 2 shows that there is not too much variation in the ellipticities and PA_{MA} 's of the outer isophotes, with the exception usually being the galaxies close to face-on and interacting systems.

5. Summary

We presented B and I band images for a sample of 88 Seyfert galaxies selected from a mostly isotropic property, the flux at $60\mu\text{m}$, as well as for an additional 20 Seyfert galaxies with extended radio emission. The isophotes of the I band images were fitted with ellipses to determine the surface brightness profiles, the ellipticities and position angles of the host galaxy major axis. The parameters obtained with these fits were used to measure the surface brightness profiles in the B band. These images were also used to measure the integrated B and I magnitudes of the galaxies. These measurements will be combined with information from radio observations to study the orientation of radio jets relative to the host galaxy disk (Kinney et al. 2000).

We would like to acknowledge the hospitality and help from the staff at CTIO, KPNO and Lick Observatories during the observations. We also would like to thank Blaise Canzian for useful comments on the measurement of ellipticities and position angles in spiral galaxies, as well as the anonymous referee for helpful comments. This work was supported by NASA grants NAGW-3757, AR-5810.01-94A, AR-6389.01-94A and the HST Director Discretionary fund D0001.82223. This research made use of the NASA/IPAC Extragalactic Database (NED), which is operated by the Jet Propulsion Laboratory, Caltech, under contract with NASA. We also used the Digitized Sky Survey, which was produced at the Space telescope Science Institute under U.S. Government grant NAGW-2166.

REFERENCES

Baum, S.A., O'Dea, C.P., de Bruyn, A.G., & Pedlar, A. 1993, ApJ, 419, 553
Brindle, C., Hough, J.H., Bailey, J.A., Axon, D.J., Ward, M.J., Sparks, W.B., & McLean, I.S. 1990, MNRAS, 244, 577
Clarke, C.J., Kinney, A.L., & Pringle, J.E. 1998, ApJ, 495, 189

De Grijp, M.H.K., Keel, W. C., Miley, G.K., Goudfrooij, P. & Lub, J. 1992, A&AS, 96, 389

De Grijp, M.H.K., Miley, G.K., & Lub, J. 1987, A&AS, 70, 95

Graham, J. A. 1982, PASP, 94, 244

Héraudeau, P., Simien, F. & Mamon, G. A. 1996, A&AS, 117, 417

Kinney, A.L., Schmitt, H.R., Clarke C.J., Pringle, J.E., Ulvestad, J.S., & Antonucci, R.R.J. 2000, ApJ, submitted

Landolt, A. U. 1992, AJ, 104, 340

Nagar, N.M., & Wilson, A.S. 1999, ApJ, 516, 97

Schmitt, H.R., Kinney, A.L., Storchi-Bergman, T., & Antonucci, R. 1997, ApJ, 477, 623

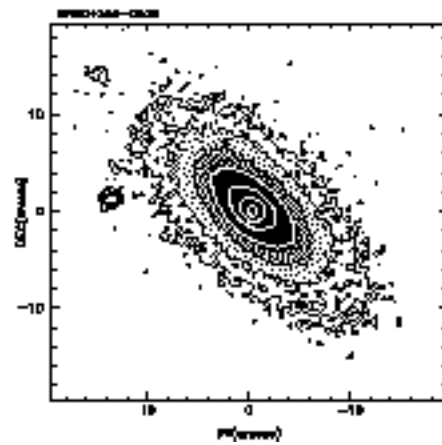
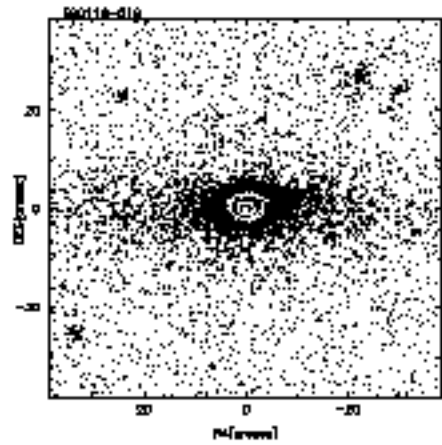
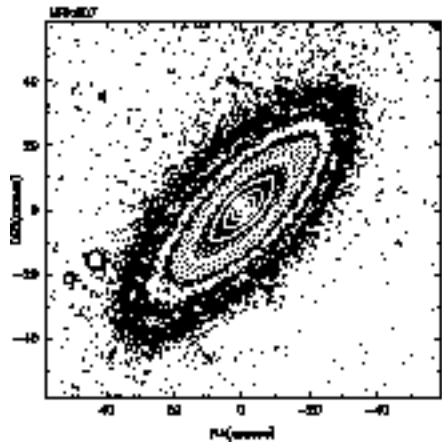
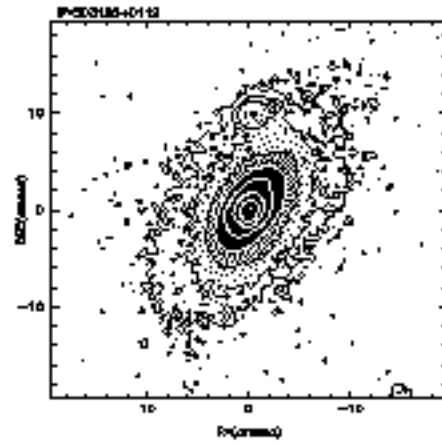
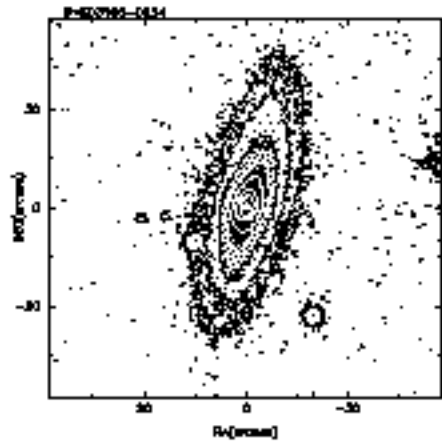
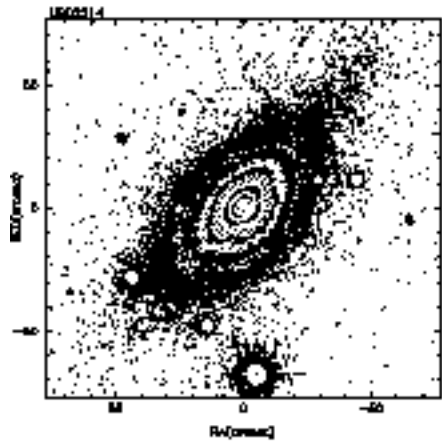
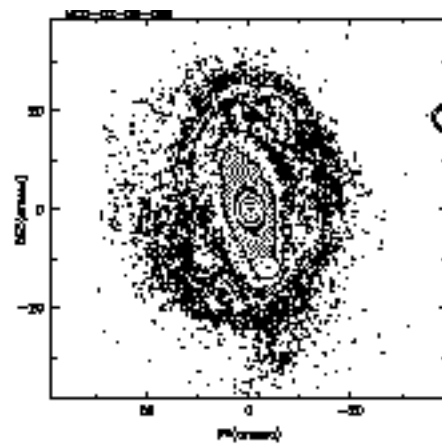
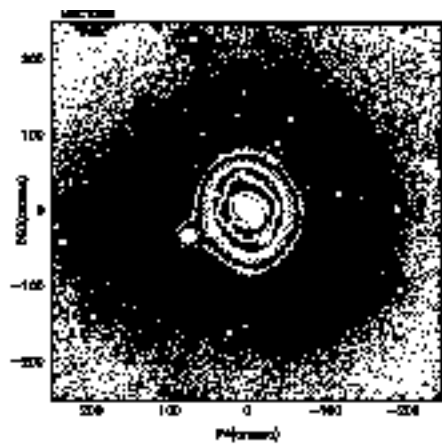
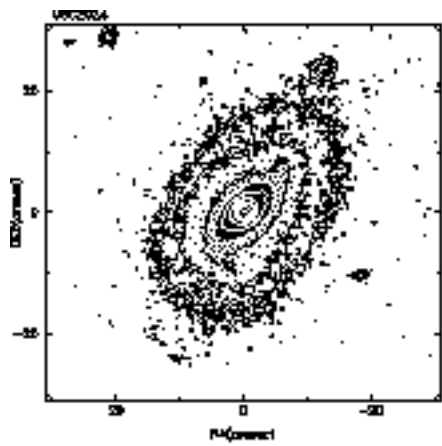
Ulvestad, J.S., & Wilson, A.S. 1984, ApJ, 285, 439

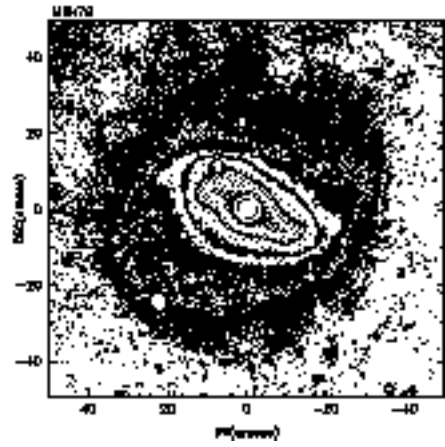
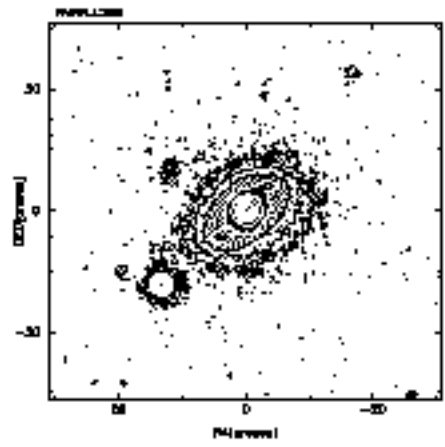
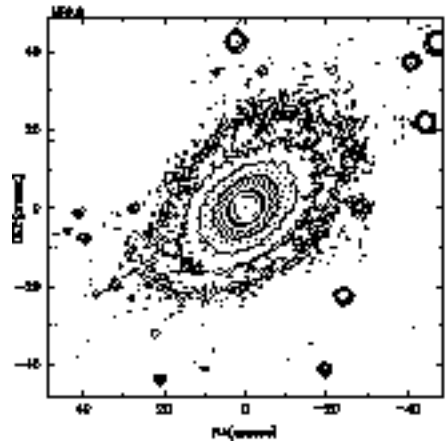
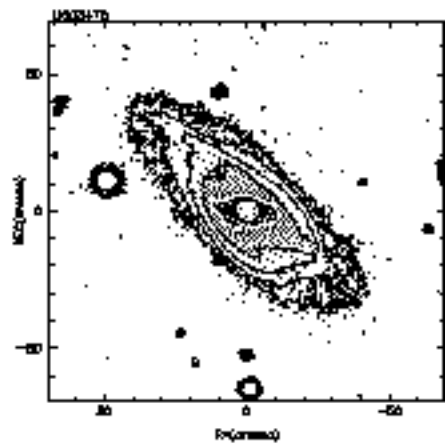
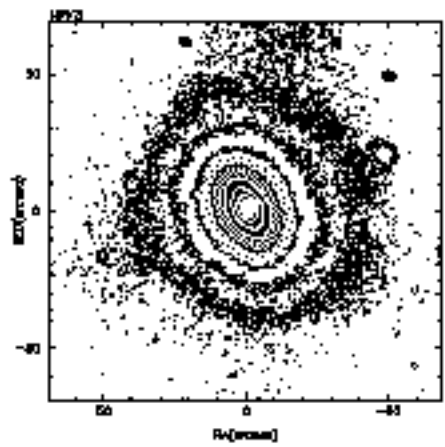
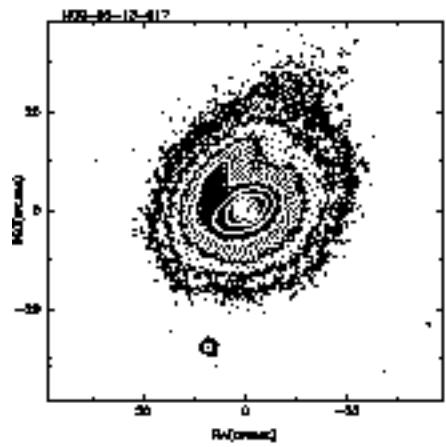
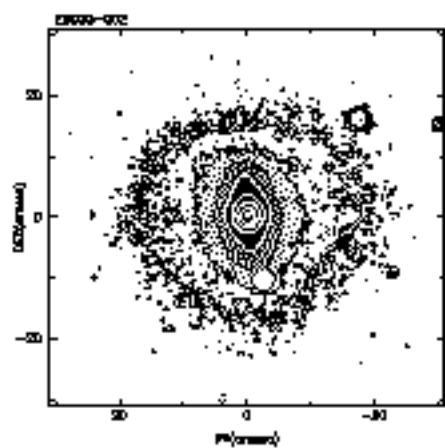
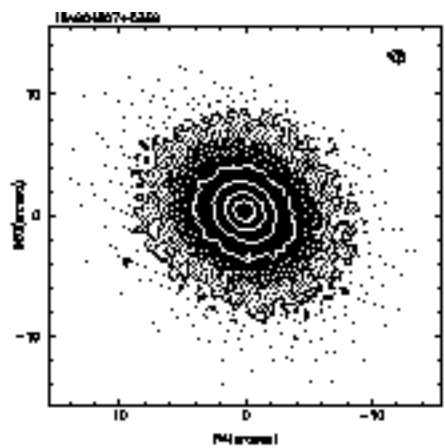
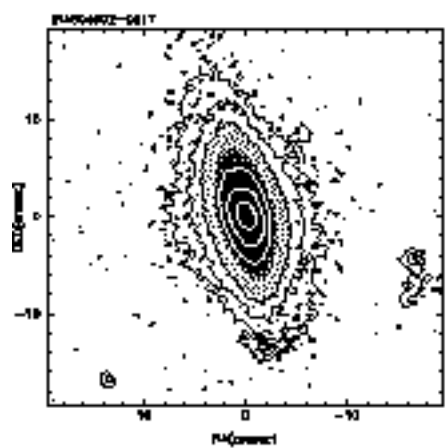
Fig. 1.— I band images of the 60 μ m sample and additional sample. In the case of UGC10683B and IRAS16382-0613, we present the B band images, because we were not able to observe them in the I band. The orientation of the images is N to the top and E to the left. The names of the galaxies are shown on the top left corner of the image which are organized following their order of appearance in Tables 1 and 2. The grayscale is a liner stretch from 0 counts (the background level) to the 19 mag arcsec⁻² surface brightness level. The contours start at 3σ above the background level, presented in Tables 4 and 5, and increase in powers of 2, times 3σ ($3\sigma \times 2^n$).

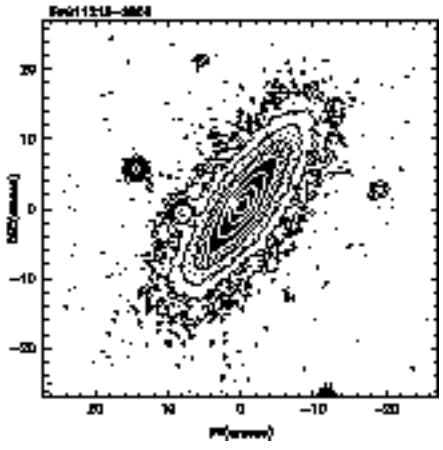
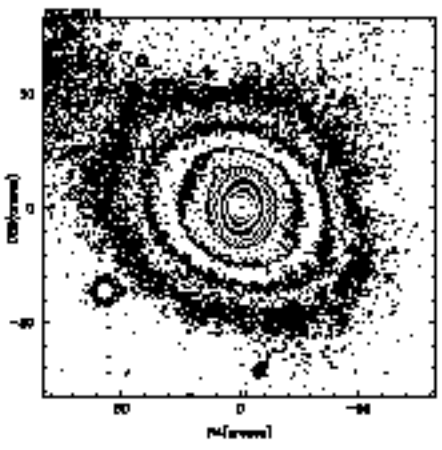
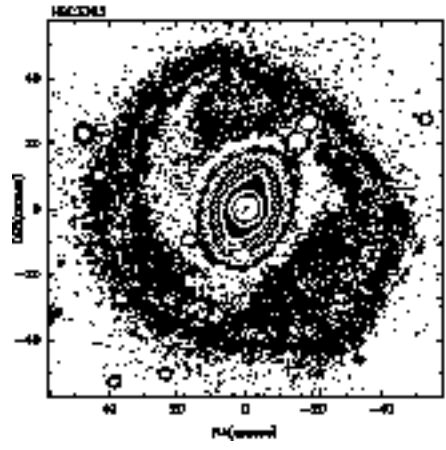
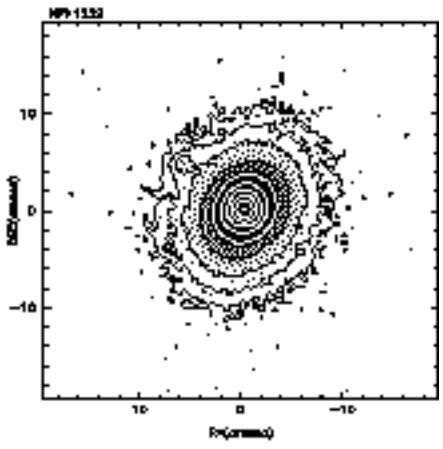
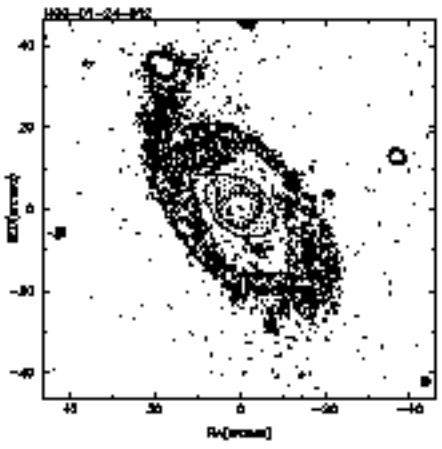
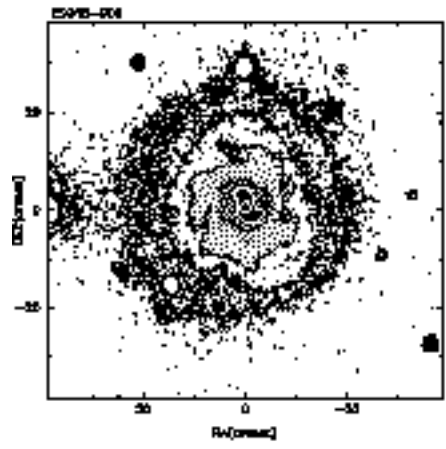
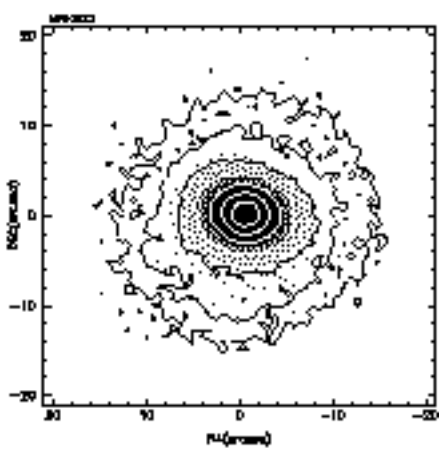
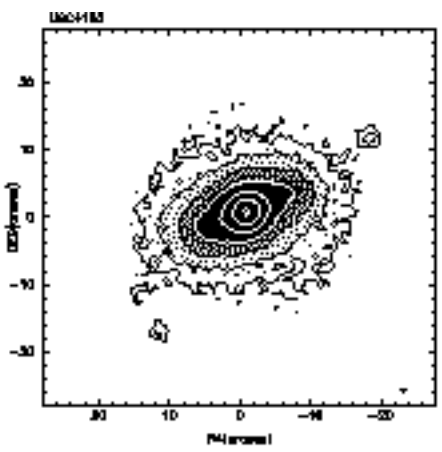
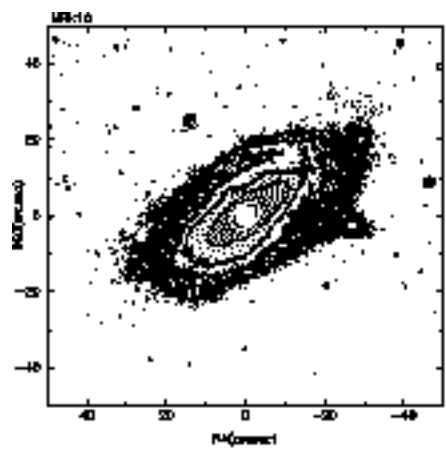
Fig. 2.— B (open triangles) and I (filled squares) surface brightness (in units of mag arcsec^{-2}), position angle of the major axis (PA_{MA}) and ellipticity (e) as a function of the semi-major axis. The position angles and ellipticities were obtained fitting ellipses to the I band images. The B surface brightness were measured using the ellipse parameters obtained from the I band images, which allow a direct comparison between the measurements in the two bands. The errorbars represent $\pm 1\sigma$ (the standard deviation).

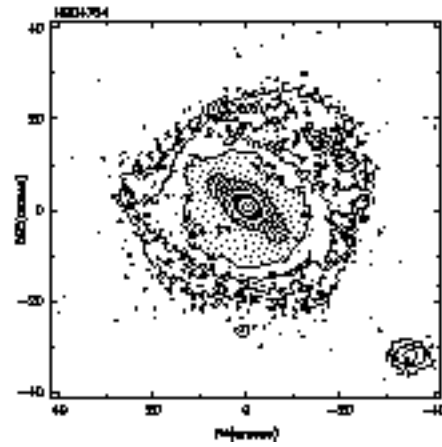
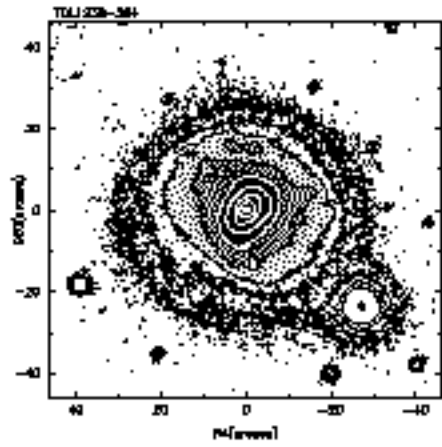
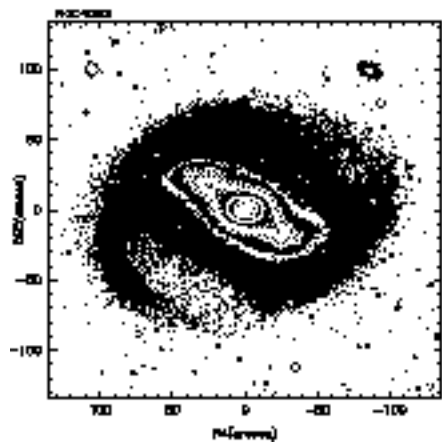
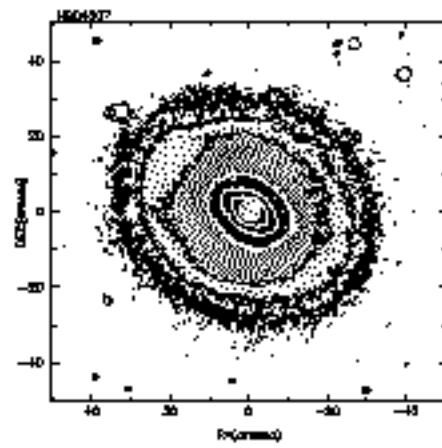
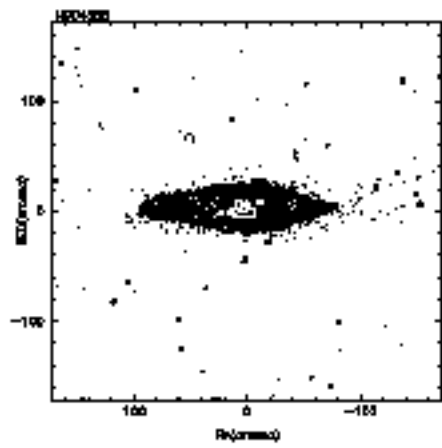
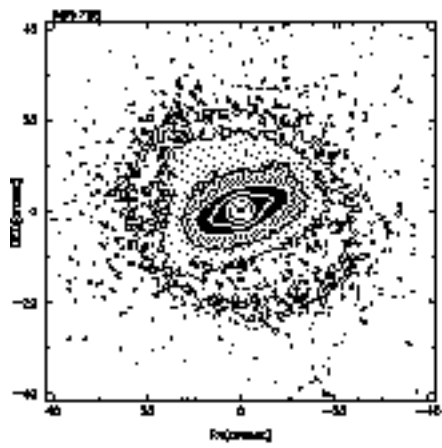
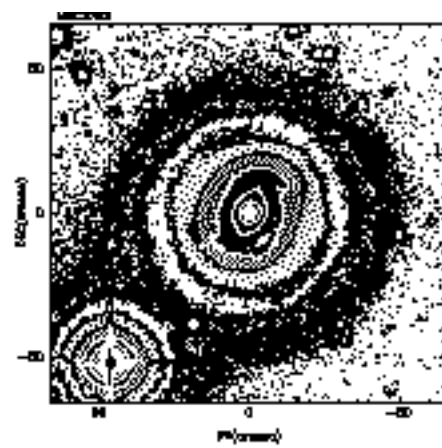
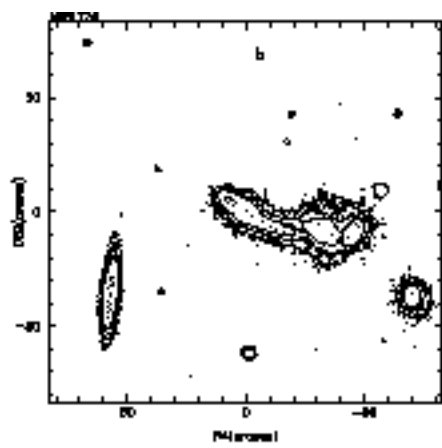
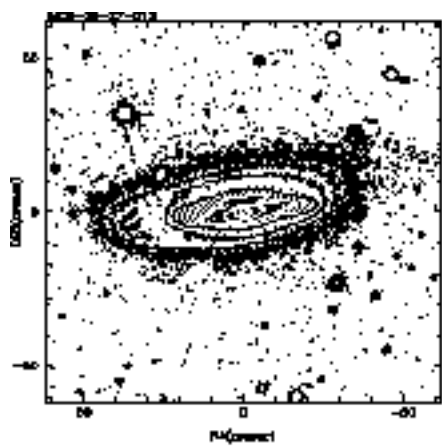
This figure "figs1.a.gif" is available in "gif" format from:

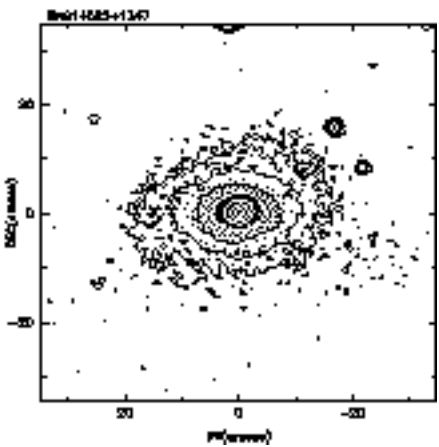
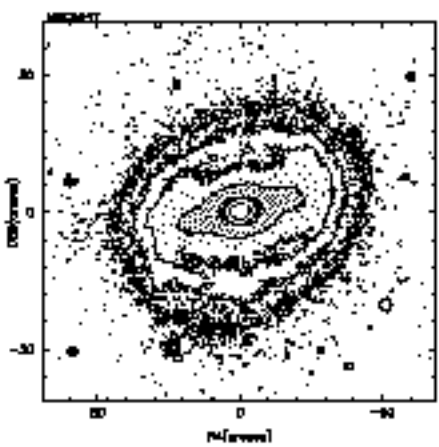
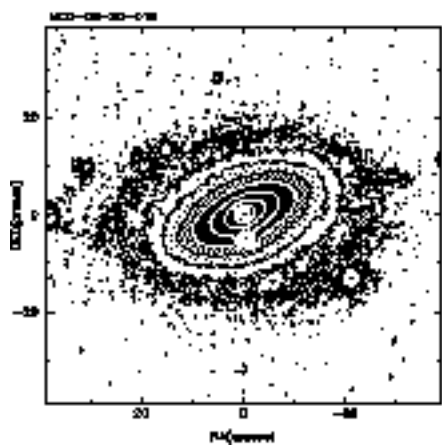
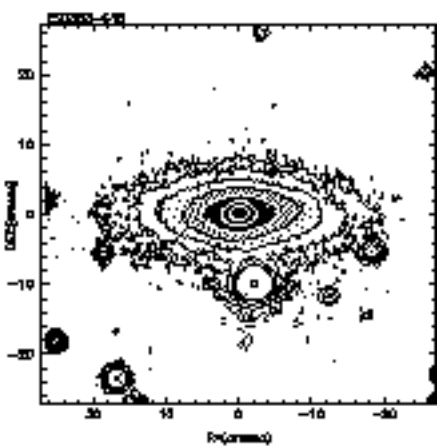
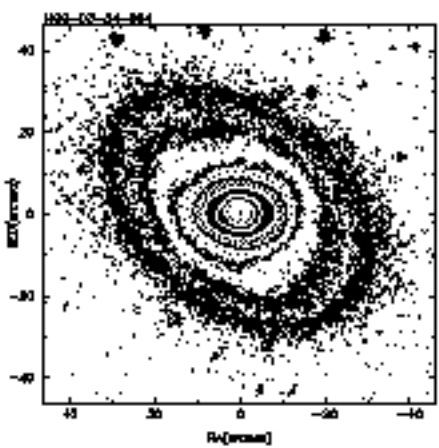
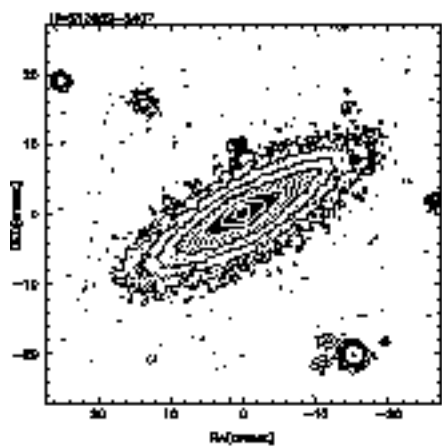
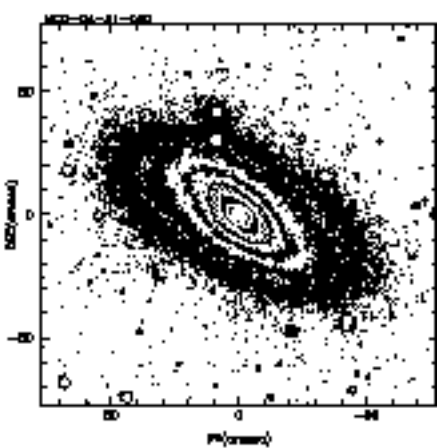
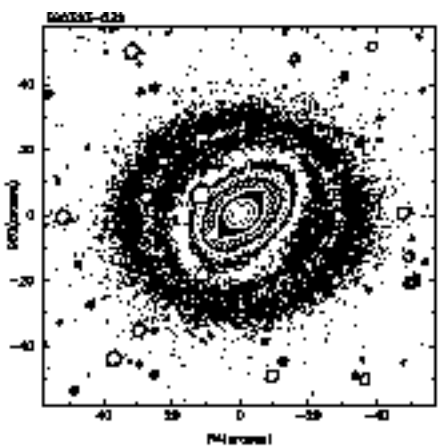
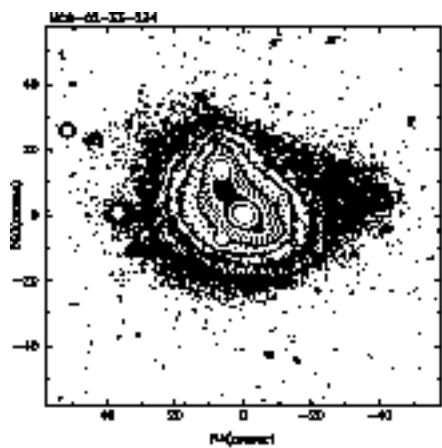
<http://arxiv.org/ps/astro-ph/0002132v1>

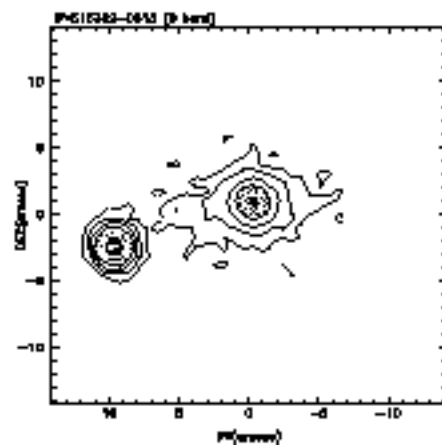
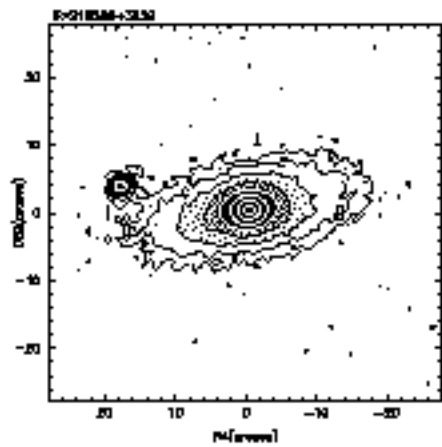
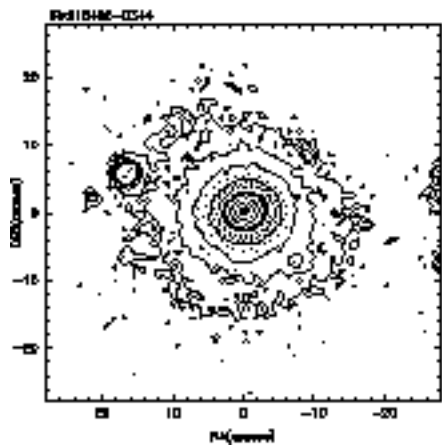
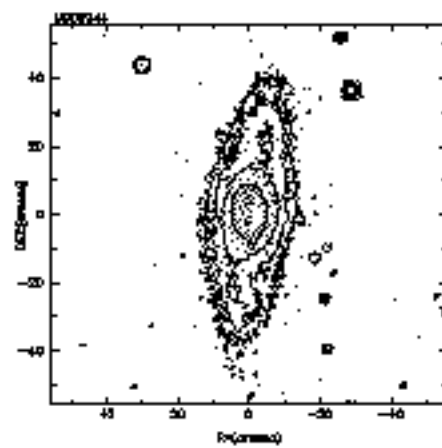
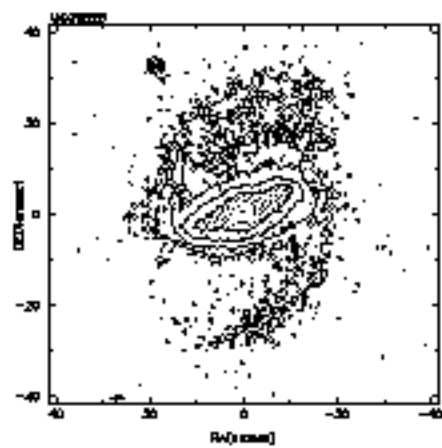
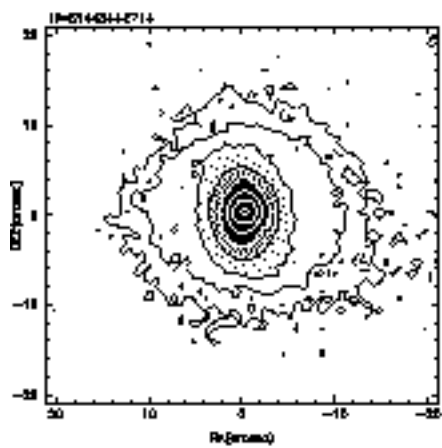
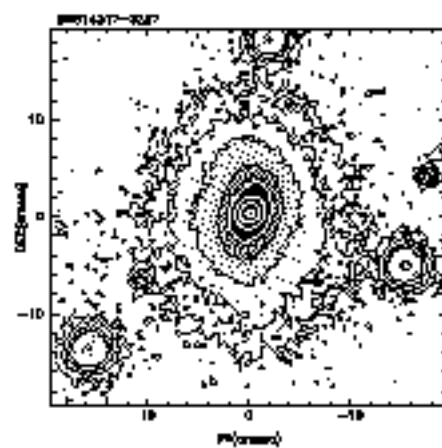
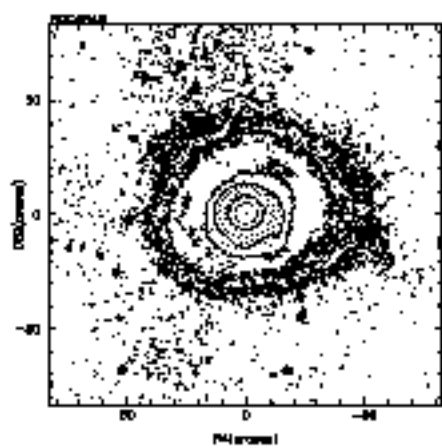
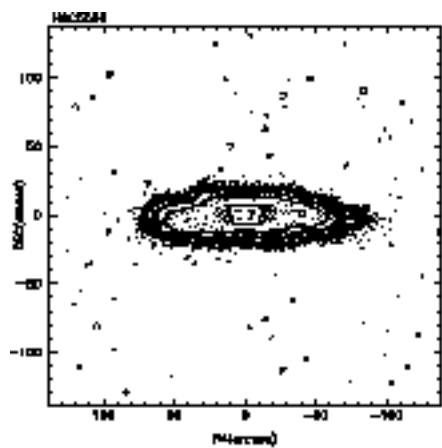


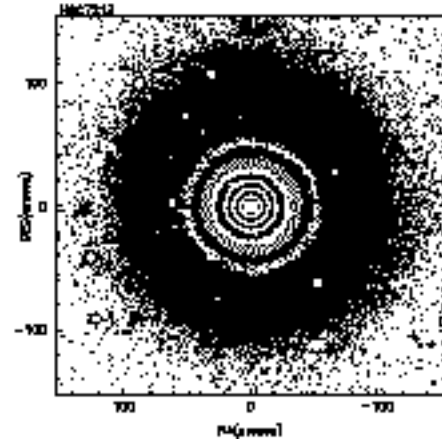
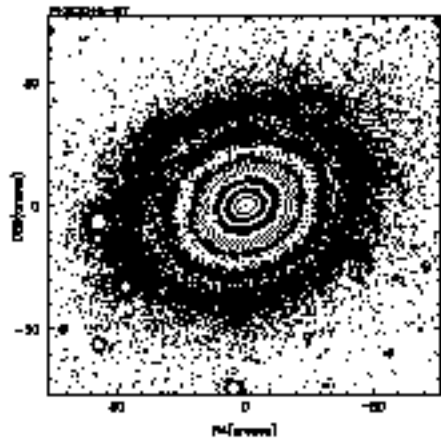
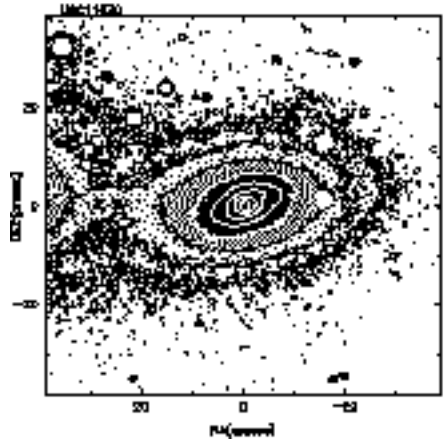
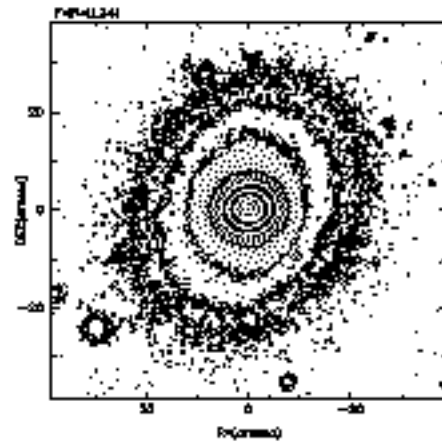
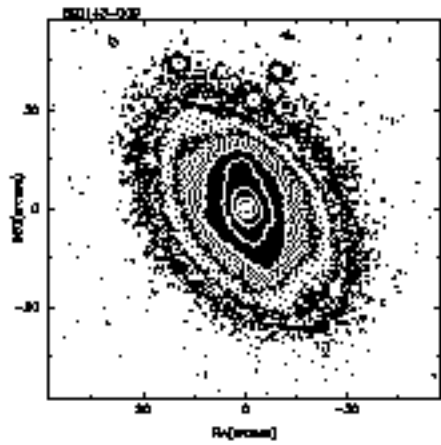
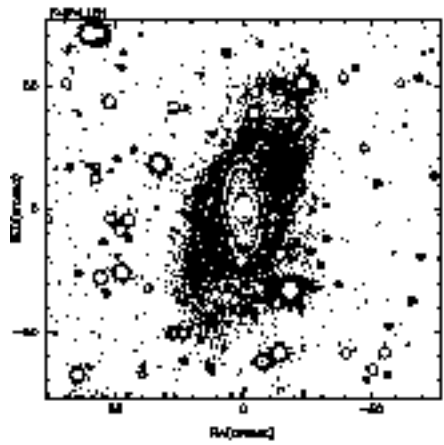
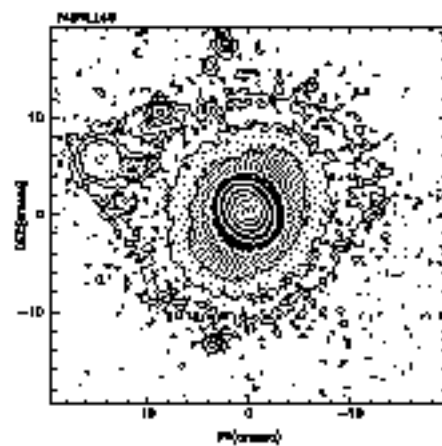
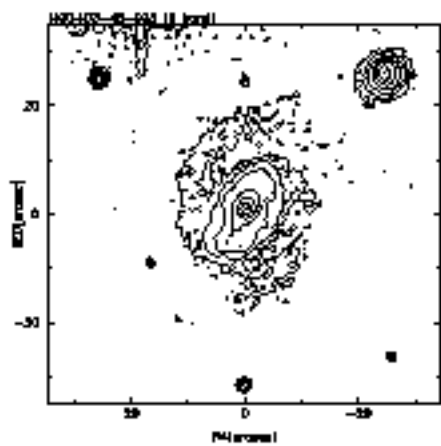
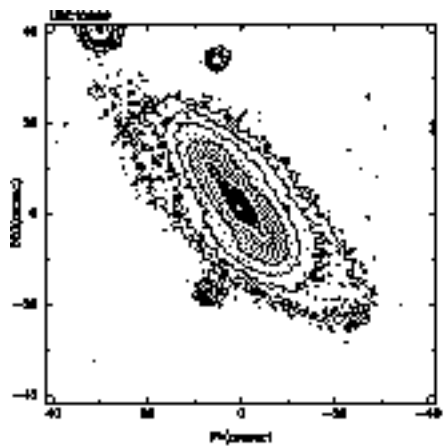


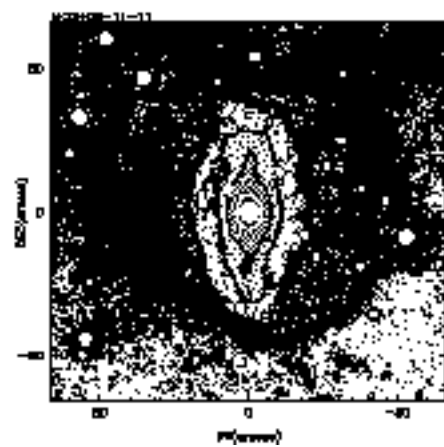
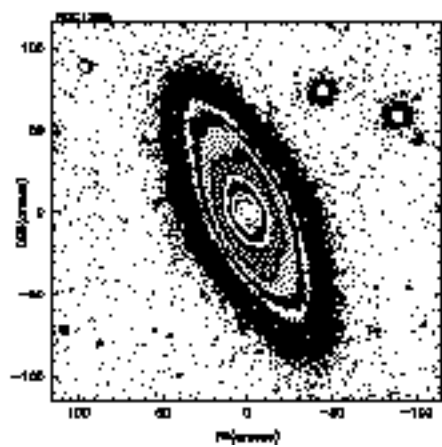
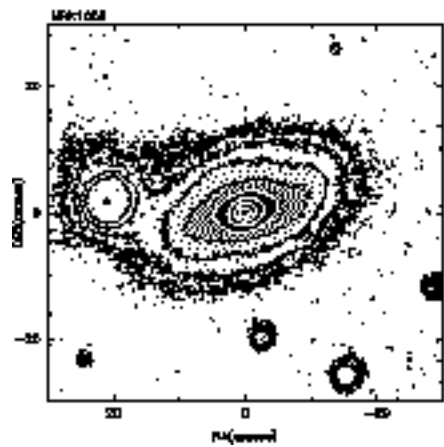
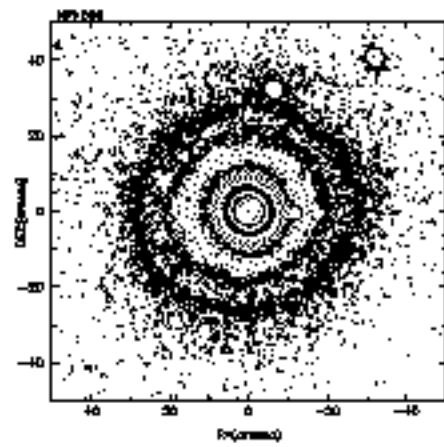
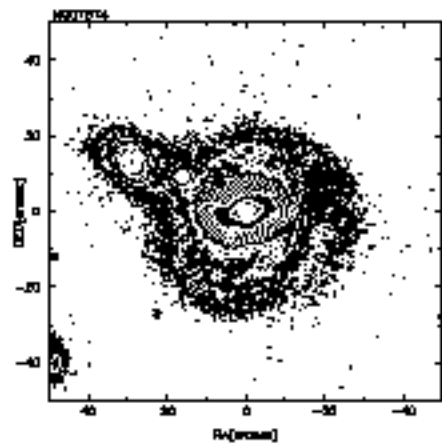
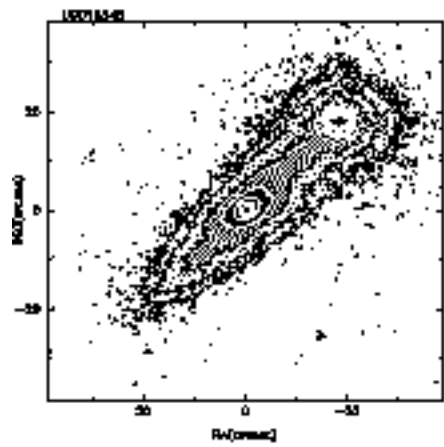
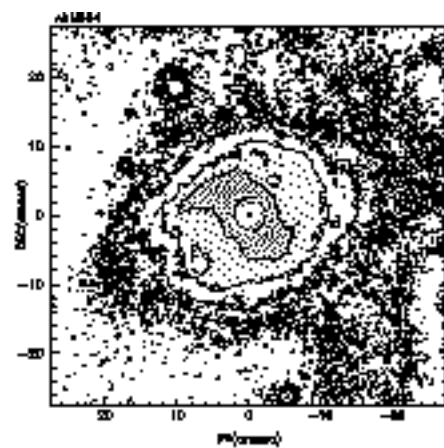
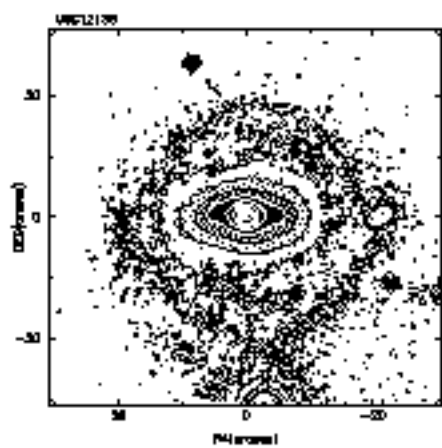
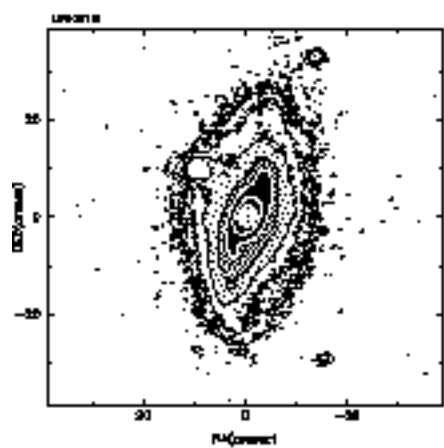


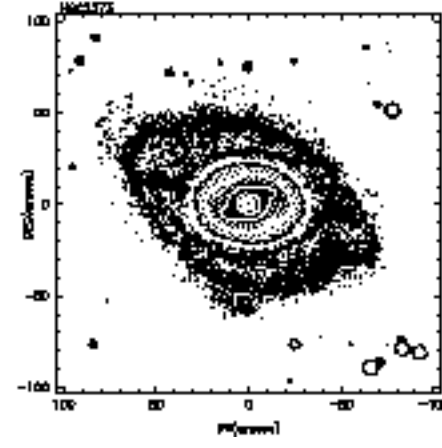
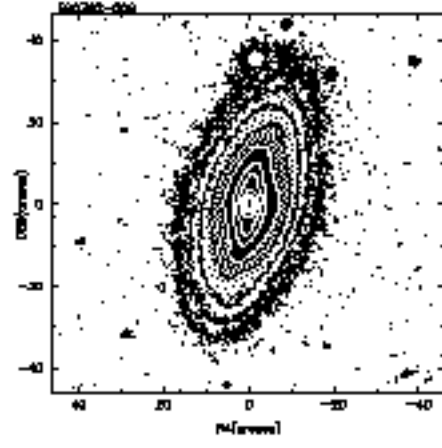
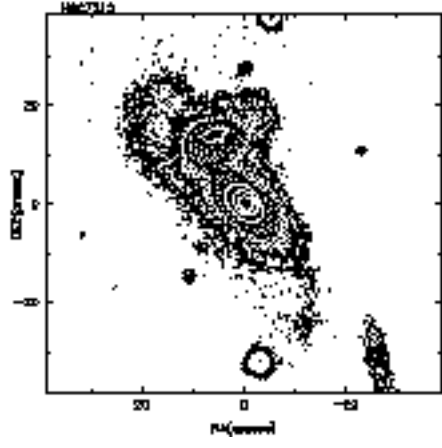
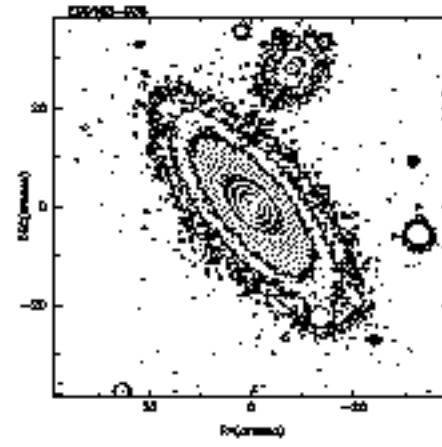
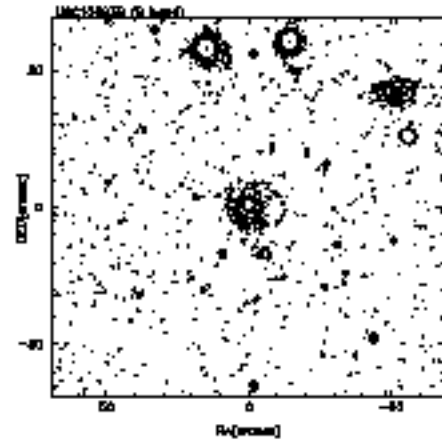
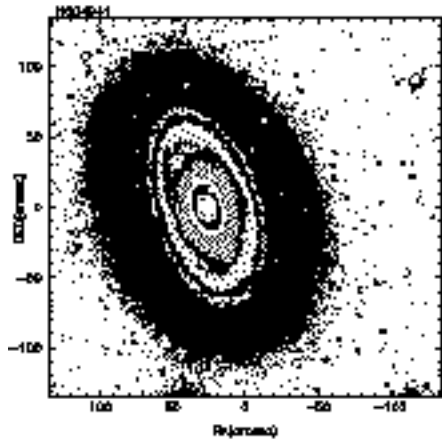
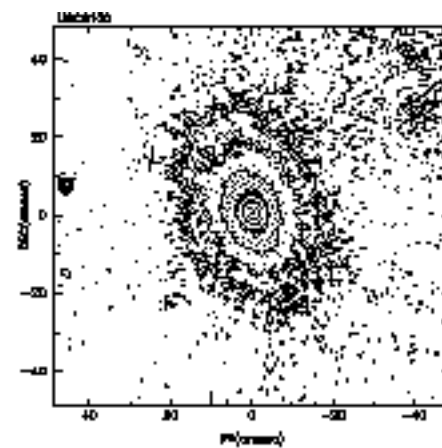
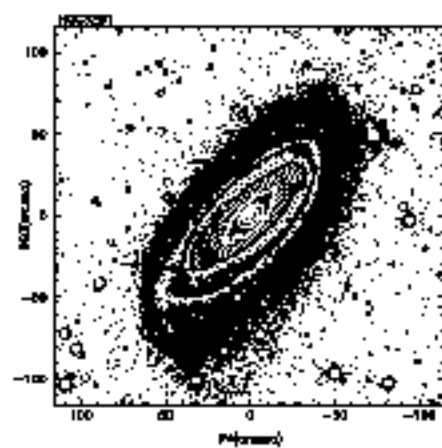
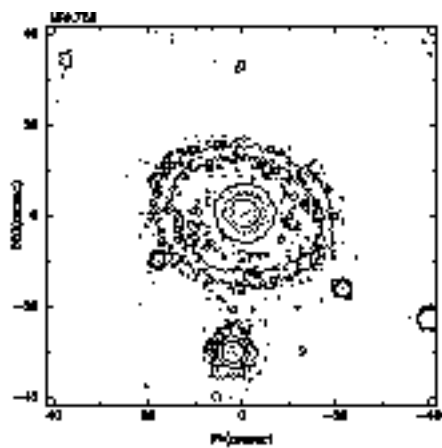


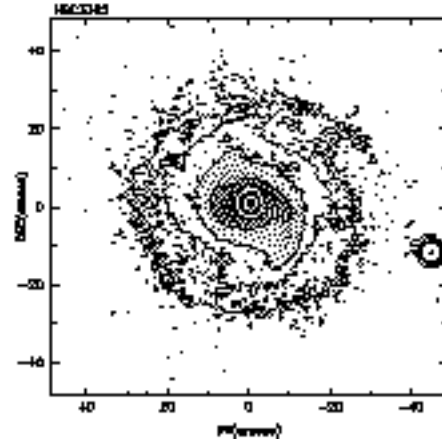
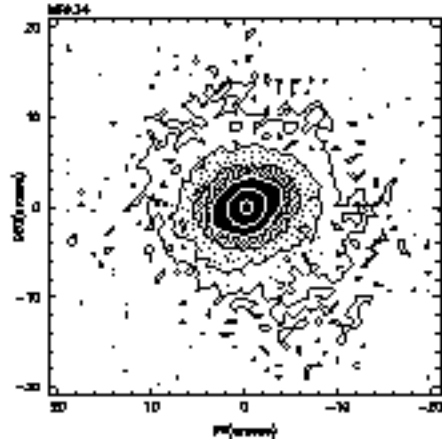
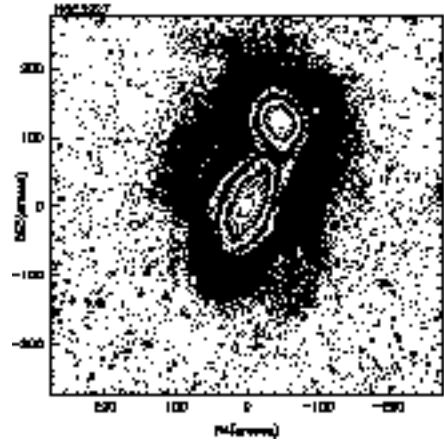
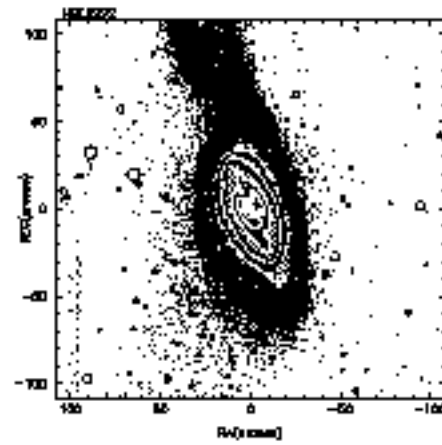
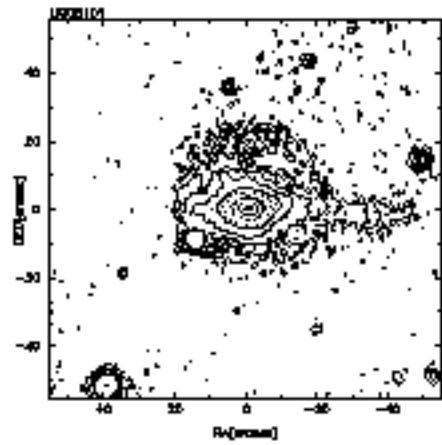
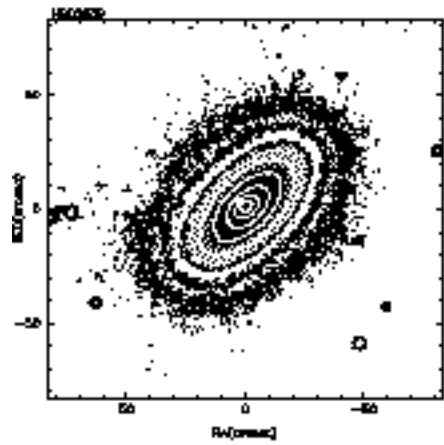
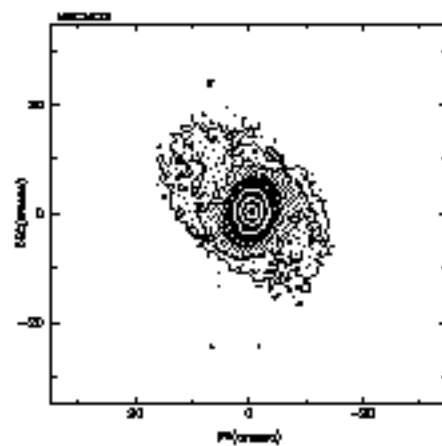
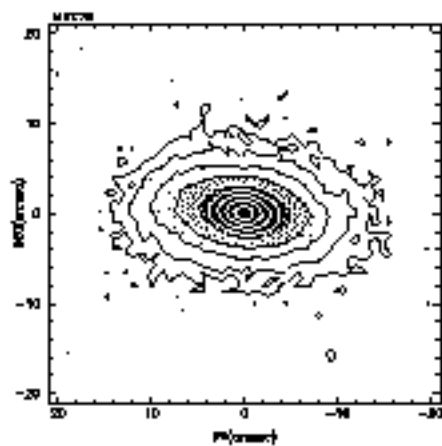
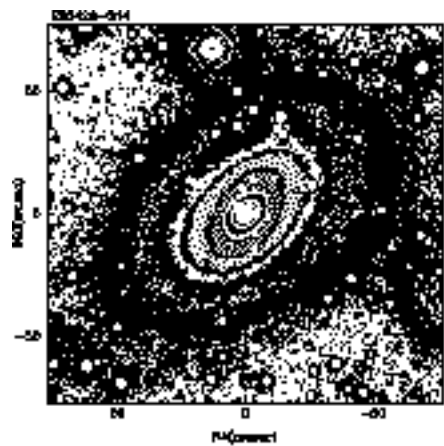


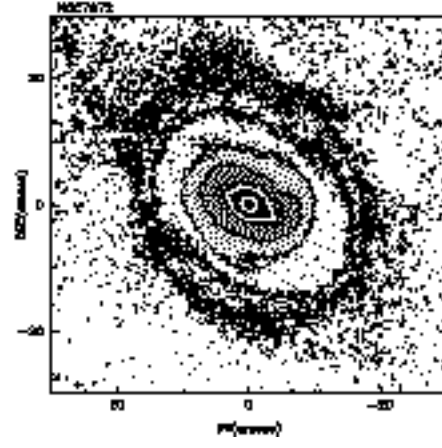
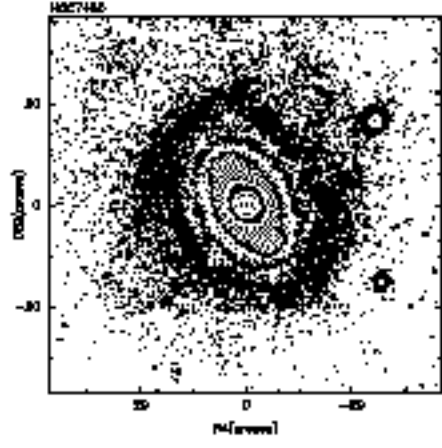
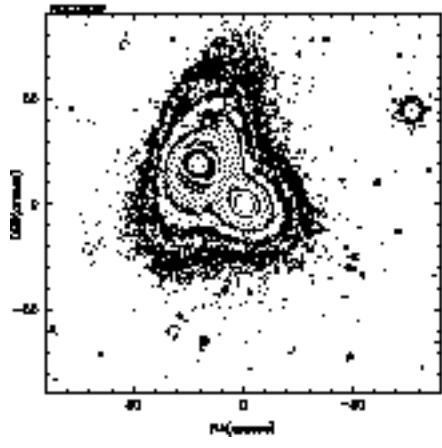
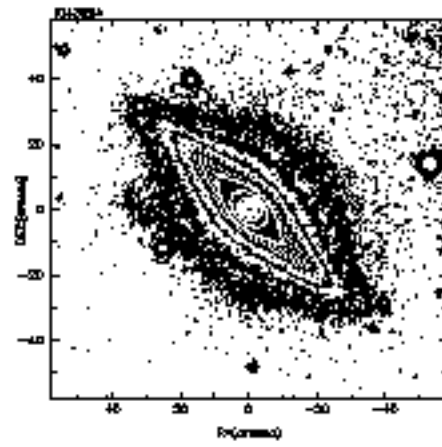
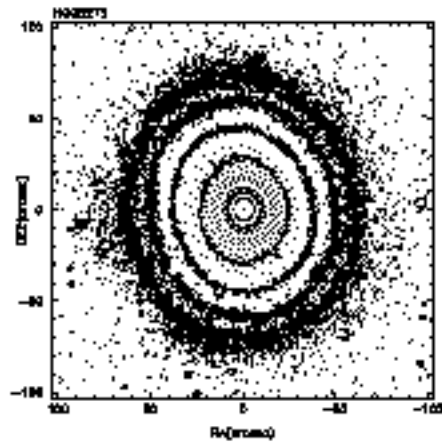
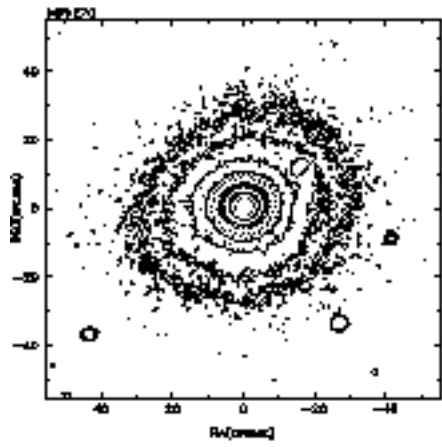
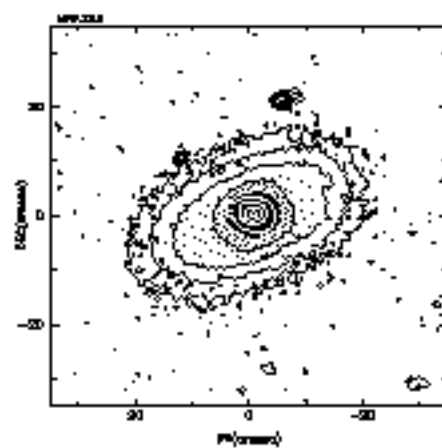
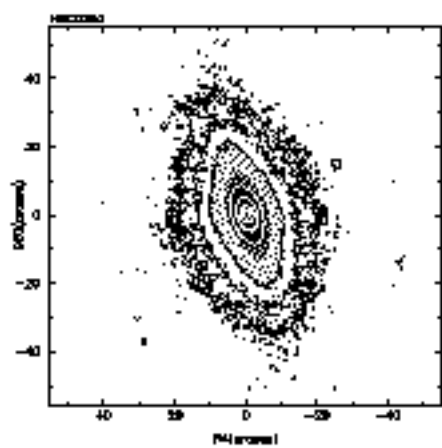
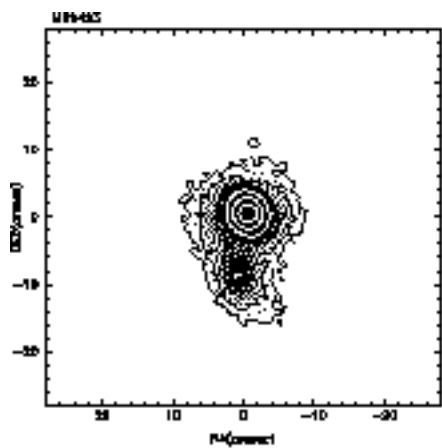












This figure "figs2a.gif" is available in "gif" format from:

<http://arxiv.org/ps/astro-ph/0002132v1>

This figure "figs2b.gif" is available in "gif" format from:

<http://arxiv.org/ps/astro-ph/0002132v1>

This figure "figs2c.gif" is available in "gif" format from:

<http://arxiv.org/ps/astro-ph/0002132v1>

This figure "figs2d.gif" is available in "gif" format from:

<http://arxiv.org/ps/astro-ph/0002132v1>

This figure "figs2e.gif" is available in "gif" format from:

<http://arxiv.org/ps/astro-ph/0002132v1>

This figure "figs2f.gif" is available in "gif" format from:

<http://arxiv.org/ps/astro-ph/0002132v1>

This figure "figs2g.gif" is available in "gif" format from:

<http://arxiv.org/ps/astro-ph/0002132v1>

This figure "figs2h.gif" is available in "gif" format from:

<http://arxiv.org/ps/astro-ph/0002132v1>

This figure "figs2i.gif" is available in "gif" format from:

<http://arxiv.org/ps/astro-ph/0002132v1>

This figure "figs2j.gif" is available in "gif" format from:

<http://arxiv.org/ps/astro-ph/0002132v1>

This figure "figs2k.gif" is available in "gif" format from:

<http://arxiv.org/ps/astro-ph/0002132v1>

This figure "figs21.gif" is available in "gif" format from:

<http://arxiv.org/ps/astro-ph/0002132v1>

This figure "figs2m.gif" is available in "gif" format from:

<http://arxiv.org/ps/astro-ph/0002132v1>

This figure "figs2n.gif" is available in "gif" format from:

<http://arxiv.org/ps/astro-ph/0002132v1>

This figure "figs2o.gif" is available in "gif" format from:

<http://arxiv.org/ps/astro-ph/0002132v1>

This figure "figs2p.gif" is available in "gif" format from:

<http://arxiv.org/ps/astro-ph/0002132v1>

This figure "figs2q.gif" is available in "gif" format from:

<http://arxiv.org/ps/astro-ph/0002132v1>

This figure "figs2r.gif" is available in "gif" format from:

<http://arxiv.org/ps/astro-ph/0002132v1>

TABLE 1
THE DATA FOR THE $60\mu\text{m}$ SAMPLE

Number	Name	Type	RA(2000)	Dec(2000)	B (s)	I (s)	Run
16	MRK 348	2	00 48 47.1	+31 57 25	1200	1200	b
24	TOL 0109-38	2	01 11 27.5	-38 05 01	720	720	a
26	MRK 1	2	01 16 07.2	+33 05 22	1800	1200	c,b
27	MRK 359	1	01 27 32.5	+19 10 44	960	960	a
33	MRK 573	2	01 43 57.8	+02 21 00	720	720	a
37	IRAS 01475-0740	2	01 50 02.7	-07 25 48	1600	2000	a
41	ESO 153-G20	2	02 06 03.6	-55 11 35	900	1200	a
47	MRK 1040	1	02 28 14.5	+31 18 42	—	1200	b
52	ESO 355-G25	2	02 31 51.0	-36 40 16	1200	1200	a
53	UGC 2024	2	02 33 01.2	+00 25 15	900	900	a
57	NGC 1068	2	02 42 40.7	-00 00 48	720	720	a
67	MCG-02-08-039	2	03 00 29.8	-11 24 59	900	900	a
68	UGC 2514	1	03 03 48.5	-01 06 13	1200	1200	a
75	IRAS 03106-0254	2	03 13 08.3	-02 43 19	1200	1200	a
78	IRAS 03125+0119	2	03 15 05.3	+01 30 30	1200	1200	a
83	MRK 607	2	03 24 48.7	-03 02 33	1600	1600	a
85	ESO 116-G18	2	03 24 53.1	-60 44 20	1600	1200	a
141	IRAS 04385-0828	2	04 40 54.9	-08 22 22	1600	1200	a
154	IRAS 04502-0317	2	04 52 44.0	-03 13 01	1600	1600	a
156	IRAS 04507+0358	2	04 53 24.9	+04 03 39	900	1600	d,a
157	ESO 33-G02	2	04 55 59.6	-75 32 27	1600	1600	a
174	MCG-05-13-017	1	05 19 35.5	-32 39 30	1600	1200	a
196	MRK 3	2	06 15 36.3	+71 02 15	900	1200	e
203	UGC 3478	1	06 32 47.3	+63 40 25	900	1200	e
209	MRK 6	1	06 52 12.3	+74 25 37	1200	1200	e
213	FAIRALL 265	1	06 56 29.7	-65 33 43	1600	1600	a
225	MRK 79	1	07 42 32.8	+49 48 35	1200	1600	b
227	MRK 10	1	07 47 29.1	+60 56 01	900	1200	b-e,e
233	UGC 4155	1	08 00 20.4	+26 36 56	1200	1200	e
236	MRK 622	2	08 07 41.0	+39 00 15	1200	1200	e
244	ESO 18-G09	2	08 24 07.4	-77 46 53	900	900	d
253	MCG-01-24-012	2	09 20 51.7	-08 04 47	900	900	d
260	MRK 1239	1	09 52 19.1	-01 36 43	900	900	d
272	NGC 3393	2	10 48 24.0	-25 09 40	900	900	d
278	NGC 3516	1	11 06 47.5	+72 34 07	1200	1200	e
281	IRAS 11215-2806	2	11 24 02.6	-28 23 15	900	900	d
282	MCG-05-27-013	2	11 27 23.3	-29 15 31	900	1200	d
283	MRK 176	2	11 32 35.3	+52 56 50	1200	1200	e
286	NGC 3783	1	11 39 01.8	-37 44 20	900	900	d
292	MRK 766	1	12 18 26.5	+29 48 46	1200	1200	e
293	NGC 4388	2	12 25 46.7	+12 39 41	1200	1200	e
299	NGC 4507	2	12 35 37.0	-39 54 31	900	900	d
301	NGC 4593	1	12 39 39.4	-05 20 39	900	900	d
302	TOL 1238-364	2	12 40 52.9	-36 45 22	900	900	d
306	NGC 4704	2	12 48 46.4	+41 55 16	1200	1200	e
309	MCG-02-33-034	1	12 52 12.4	-13 24 54	900	900	d
310	ESO 323-G32	2	12 53 19.8	-41 38 14	900	900	d
313	MCG-04-31-030	2	13 07 06.0	-23 40 43	900	900	d
314	IRAS 13059-2407	2	13 08 42.1	-24 23 00	900	900	d
317	MCG-03-34-064	2	13 22 24.4	-16 43 43	900	900	d
322	ESO 383-G18	2	13 33 26.3	-34 00 59	900	900	d
324	MCG-6-30-15	1	13 35 53.7	-34 17 45	900	900	d
329	NGC 5347	2	13 53 17.8	+33 29 27	900	1200	e
340	IRAS 14082+1347	2	14 10 41.4	+13 33 29	1200	1200	e
341	NGC 5506	2	14 13 14.8	-03 12 27	900	1200	e
344	NGC 5548	1	14 17 59.5	+25 08 12	900	1200	e
349	IRAS 14317-3237	2	14 34 44.9	-32 50 28	900	900	d
354	IRAS 14434+2714	2	14 45 36.8	+27 02 05	1200	1200	e
369	UGC 9826	1	15 21 33.0	+39 12 01	900	1200	e
377	UGC 9944	2	15 35 47.8	+73 27 02	1200	1200	e
383	IRAS 15480-0344	2	15 50 41.5	-03 53 18	1200	1200	e
409	IRAS 16288+3929	2	16 30 32.6	+39 23 03	1200	1200	e
418	IRAS 16382-0613	2	16 40 52.3	-06 18 52	1200	—	a-e
445	UGC 10889	2	17 30 20.7	+59 38 20	1200	900	e
447	MCG+03-45-003	2	17 35 32.7	+20 47 48	1200	1200	e
471	FAIRALL 49	2	18 36 58.1	-59 24 09	1200	720	a
473	FAIRALL 51	1	18 44 54.3	-62 21 49	1200	1500	a
497	ESO 143-G09	1	20 08 46.1	-61 05 56	900	900	a

TABLE 1—*Continued*

Number	Name	Type	RA(2000)	Dec(2000)	B (s)	I (s)	Run
501	FAIRALL 341	2	20 19 59.0	−52 37 20	1600	1200	a
510	UGC 11630	2	20 47 33.5	+00 24 42	720	720	a
512	PKS 2048−57	2	20 52 02.0	−57 04 09	900	900	a
530	NGC 7213	1	22 09 16.2	−47 10 00	900	900	a
537	MRK 915	1	22 36 46.5	−12 32 43	1200	1200	a
538	UGC 12138	1	22 40 17.0	+08 03 14	1600	1600	a
540	AKN 564	1	22 42 39.3	+29 43 31	1200	1200	b
549	UGC 12348	2	23 05 19.4	+00 11 28	1200	1600	a
555	NGC 7674	2	23 27 56.7	+08 46 45	1200	1200	a
590	MRK 590	1	02 14 33.6	−00 46 00	1600	1600	a
594	MRK 1058	2	02 49 51.8	+34 59 17	1800	1200	c,b
602	NGC 1386	2	03 36 45.4	−35 59 57	1200	1200	a
615	MCG +8-11-11	1	05 54 53.6	+46 26 22	1200	1200	b
627	MRK 705	1	09 26 03.3	+12 44 04	1200	1200	e
634	NGC 3281	2	10 31 52.1	−32 51 13	900	900	d
638	UGC 6100	2	11 01 34.0	+45 39 14	1200	1200	e
665	NGC 4941	2	13 04 13.1	−05 33 06	900	900	d
703	UGC 10683B	1	17 05 00.4	−01 32 29	1200	—	e
708	ESO 103-G35	2	18 38 20.3	−65 25 42	720	720	a
721	NGC 7212	2	22 07 02.0	+10 14 00	1200	1200	a

Column 1 shows the galaxy number in the de Grijp et al. (1987) catalogue, Column 2 shows their names and Column 3 the Seyfert type. Columns 4 and 5 give the Right Ascension and Declination, respectively. Columns 6 and 7 give the total exposure time of the B and I images, respectively. Column 8 shows the observing run when the galaxies were imaged, according to the code given in Table 1.

TABLE 2
THE ADDITIONAL SAMPLE

Name	Type	RA(2000)	Dec(2000)	B (s)	I (s)	Run	Comments
NGC 235A	1	00 42 52.8	-23 32 29	-	-	-	interacting
NGC 513	2	01 24 26.9	+33 47 58	-	-	-	
NGC 526A	1	01 23 54.2	-35 03 55	-	-	-	interacting
NGC 591	2	01 33 31.3	+35 40 05	-	-	-	
NGC 788	2	02 01 06.4	-06 48 56	-	-	-	not extended in radio
NGC 1144	2	02 55 12.2	-00 11 01	-	-	-	merger
ESO 417-G6	2	02 56 21.5	-32 11 06	-	-	-	not extended in radio
MRK 1066	2	02 59 58.6	+36 49 14	-	-	-	
NGC 1365	1	03 33 36.4	-36 08 25	-	-	-	
MRK 618	1	04 36 22.2	-10 22 34	-	-	-	
ESO 362-G8	2	05 11 09.0	-34 23 36	900	900	d	
NGC 2110	2	05 52 11.4	-07 27 22	-	-	-	
NGC 2273	2	06 50 08.7	+60 50 45	800	1200	e	
ESO 428-G14	2	07 14 32.9	-29 14 04	900	900	d	
MRK 78	2	07 42 41.7	+65 10 37	1200	1200	e	
NGC 2622	1	08 38 10.9	+24 53 43	1200	1200	e	
NGC 2639	1	08 43 38.0	+50 12 20	1200	1200	e	
MRK 110	1	09 25 12.9	+52 17 11	-	-	-	merger
UGC 5101	1	09 35 51.6	+61 21 11	1200	800	e	merger
NGC 2992	2	09 45 42.0	-14 19 35	-	900	d	interacting
NGC 3081	2	09 59 29.5	-22 49 35	-	-	-	not extended in radio
NGC 3227	1	10 23 30.6	+19 51 54	-	1600	e	
MRK 34	2	10 34 08.6	+60 01 52	-	900	e	
NGC 3362	2	10 44 51.7	+06 35 48	-	900	e	interacting
MRK 423	2	11 26 48.5	+35 15 03	-	900	e	merger
NGC 4051	1	12 03 09.6	+44 31 53	-	-	-	
NGC 4074	2	12 04 29.7	+20 18 59	-	-	-	not extended in radio
NGC 4117	2	12 07 46.1	+43 07 35	-	-	-	
NGC 4151	1	12 10 32.6	+39 24 21	-	-	-	
MRK 231	1	12 56 14.2	+56 52 25	-	-	-	merger
ESO 323-G77	1	13 06 26.6	-40 24 50	-	-	-	
NGC 5135	2	13 25 44.0	-29 50 02	-	-	-	
NGC 5252	2	13 38 16.0	+04 32 33	-	1200	e	
MRK 266	2	13 38 17.7	+48 16 34	-	-	-	merger
MRK 268	2	13 41 11.1	+30 22 41	-	1200	e	
MRK 270	2	13 41 05.8	+67 40 20	1200	1200	e	
NGC 5273	1	13 42 08.3	+35 39 15	1200	1200	e	
MRK 273	2	13 44 42.1	+55 53 13	-	-	-	merger
IC 4329A	1	13 49 19.3	-30 18 34	-	720	d	
MRK 279	1	13 53 03.4	+69 18 30	-	-	-	
MRK 463E	2	13 56 02.9	+18 22 19	-	-	-	merger
NGC 5643	2	14 32 40.7	-44 10 29	-	-	-	
NGC 5728	2	14 42 23.9	-17 15 11	-	-	-	
NGC 5929	2	15 26 06.2	+41 40 14	1200	1200	e	interacting
ESO 137-G34	2	16 35 14.2	-58 04 41	-	-	-	
MRK 509	1	20 44 09.7	-10 43 25	-	-	-	
NGC 7172	2	22 02 01.7	-31 52 18	-	-	-	
IC 5169	2	22 10 10.0	-36 05 18	-	-	-	
NGC 7450	1	23 00 47.8	-12 55 07	-	1200	b	
NGC 7465	2	23 02 00.9	+15 57 53	-	-	-	
MRK 926	1	23 04 43.5	-08 41 08	-	-	-	
NGC 7672	2	23 27 31.4	+12 23 06	-	900	b	
NGC 7743	2	23 44 21.5	+09 56 05	-	-	-	

Column 1 gives the galaxy name and Column 2 the Seyfert type. Columns 3 and 4 give the Right Ascension and Declination, respectively. Columns 5 and 6 give the total exposure time of the B and I images, respectively. Column 7 shows the observing run when the galaxies were imaged, according to the code given in Table 1. For those galaxies which will not be used in future analysis, we give in Column 8 the reason to exclude them.

TABLE 3
OBSERVING RUNS

Date	Telescope	f-ratio	Instrument	FOV '	Scale "/pixel	Code
October 03-09/10 1998	CTIO 0.9m	13.5	CCD Direct T2K6	13.0	0.384	a
November 13-18/19 1998	Lick 1.0m	17.0	CCD Direct CCD #5	4.8	0.248	b
December 17-21/22 1998	Lick 1.0m	17.0	CCD Direct CCD #5	4.8	0.248	c
February 10-12/13 1999	CTIO 0.9m	13.5	CCD Direct T2K3	7.5	0.384	d
April 23-29/30 1999	KPNO 0.9m	7.5	CCD Direct T2KA	11.7	0.688	e

TABLE 4
MAGNITUDES OF THE $60\mu\text{m}$ SAMPLE

Name	Aperture B (arcsec)	$3\sigma B$ (mag arcsec $^{-2}$)	B (mag)	(seeing B) (arcsec)	Aperture I (arcsec)	$3\sigma I$ (mag arcsec $^{-2}$)	I (mag)	(seeing I) (arcsec)
MRK 348	39.7	23.80	14.96	0.9	42.7	22.56	12.87	0.9
TOL 0109-38	46.1	22.18	13.84	1.2	84.5	22.13	11.67	1.0
MRK 1	27.8	24.04	15.62	2.6	31.7	22.69	13.52	1.1
MRK 359	23.0	22.67	14.44	1.4	32.3	21.65	12.57	1.2
MRK 573	24.6	23.08	14.66	1.2	36.9	21.92	12.43	1.0
IRAS 01475-0740	16.9	24.52	16.58	2.7	20.0	23.03	14.46	1.2
ESO 153-G20	30.7	22.40	15.09	1.3	76.8	22.35	12.10	1.1
MRK 1040	—	—	—	—	123.0	22.56	11.73	1.5
ESO 355-G25	49.2	23.60	14.00	2.6	49.2	21.65	12.02	1.0
UGC 2024	26.1	23.19	15.26	1.3	43.0	22.26	13.02	1.2
NGC 1068	192.0	22.84	9.93	1.5	318.7	21.86	7.73	1.3
MCG-02-08-039	33.8	23.07	15.57	1.2	56.8	21.99	12.80	1.3
UGC 2514	32.3	22.79	14.96	1.5	92.2	22.14	11.74	1.2
IRAS 03106-0254	20.0	22.61	16.37	1.5	58.4	22.45	12.86	1.2
IRAS 03125+0119	15.4	22.90	15.87	1.4	32.3	22.16	13.46	1.4
MRK 607	81.4	23.60	13.79	2.7	101.4	22.45	11.41	1.5
ESO 116-G18	36.9	23.36	15.36	2.5	33.8	20.54	12.85	1.3
IRAS 04385-0828	18.4	22.57	16.19	1.0	35.3	22.15	13.52	1.0
IRAS 04502-0317	20.0	23.16	15.92	2.5	30.7	22.64	13.65	1.2
IRAS 04507+0358	36.9	24.18	15.25	1.6	27.7	21.79	13.02	1.2
ESO 33-G02	30.7	23.58	15.13	2.5	43.0	21.83	12.58	1.2
MCG-05-13-017	43.0	23.59	13.60	1.7	44.5	22.08	11.94	1.2
MRK 3	53.7	23.99	13.94	1.7	82.6	22.29	11.28	1.3
UGC 3478	62.8	23.43	14.11	1.6	111.5	22.98	11.83	1.9
MRK 6	111.5	22.98	11.83	1.8	67.4	22.77	12.22	1.3
FAIRALL 265	29.2	23.48	14.99	2.0	46.1	22.29	13.11	1.1
MRK 79	47.6	23.91	14.39	1.1	77.4	22.76	12.10	1.0
MRK 10	64.7	23.67	14.45	1.8	92.2	23.15	12.43	1.3
UGC 4155	30.3	23.41	14.92	2.4	45.4	21.87	12.60	1.9
MRK 622	27.5	23.10	14.96	1.8	30.3	22.45	13.40	2.1
ESO 18-G09	49.2	24.17	14.45	1.3	45.3	22.07	12.88	1.3
MCG-01-24-012	66.1	24.38	15.00	1.3	61.4	22.60	13.16	1.1
MRK 1239	21.5	24.41	15.19	1.3	23.8	22.75	13.21	1.4
NGC 3393	92.2	24.16	13.19	1.3	90.6	22.11	11.04	0.9
NGC 3516	83.9	23.83	12.78	1.9	103.2	22.13	10.68	1.9
IRAS 11215-2806	30.7	23.85	15.58	1.1	30.7	21.53	13.43	1.1
MCG-05-27-013	79.9	24.50	14.96	1.1	92.2	23.01	12.27	1.0
MRK 176	31.7	23.50	15.18	1.8	41.3	22.28	13.21	1.6
NGC 3783	106.0	24.31	12.62	1.3	86.8	22.08	10.77	1.0
MRK 766	46.8	23.60	13.96	1.7	55.0	22.15	12.08	1.7
NGC 4388	227.0	23.66	12.11	1.8	192.6	21.90	10.38	1.7
NGC 4507	76.8	24.02	13.11	1.1	69.1	21.83	11.12	0.9
NGC 4593	179.7	24.25	12.12	1.3	216.6	22.88	9.97	1.3
TOL 1238-364	61.4	23.94	13.03	1.3	61.4	22.46	11.52	1.7
NGC 4704	45.4	23.91	14.73	1.9	56.4	22.76	12.68	1.6
MCG-02-33-034	96.0	23.90	13.71	1.1	96.0	22.39	11.73	1.3
ESO 323-G32	58.4	24.15	13.85	1.3	73.7	22.56	11.53	1.1
MCG-04-31-030	87.6	24.23	14.24	1.3	115.2	22.81	11.70	1.0
IRAS 13059-2407	32.3	24.27	16.55	1.1	41.5	23.20	14.01	0.9
MCG-03-34-064	46.9	24.13	14.44	0.9	73.7	22.73	11.83	1.1
ESO 383-G18	27.7	23.26	15.63	1.4	30.7	22.08	13.92	1.5
MCG-6-30-15	44.5	23.95	14.11	1.1	50.7	22.41	11.87	1.1
NGC 5347	79.8	23.90	13.61	1.7	100.4	22.99	11.58	1.4
IRAS 14082+1347	26.1	23.19	15.64	1.4	38.5	22.25	13.42	1.3
NGC 5506	148.6	23.62	13.14	1.7	166.5	22.33	10.94	1.5
NGC 5548	99.1	24.79	13.04	1.7	112.8	23.47	11.43	1.5
IRAS 14317-3237	23.0	24.05	16.33	1.0	30.7	22.69	13.91	1.2
IRAS 14434+2714	27.5	24.30	15.73	1.6	26.1	22.38	14.02	1.5
UGC 9826	55.0	24.39	15.11	1.6	66.1	23.00	13.02	1.1
UGC 9944	63.3	23.65	14.99	1.5	78.4	22.74	12.77	1.2
IRAS 15480-0344	20.6	24.32	16.32	1.3	37.2	22.98	13.45	1.4
IRAS 16288+3929	30.3	23.93	15.62	1.2	39.9	22.80	13.55	1.6
IRAS 16382-0613	19.3	23.32	16.60	1.3	—	—	—	—
UGC 10889	74.3	25.54	14.97	1.2	71.6	22.95	12.88	2.3
MCG+03-45-003	35.8	24.20	15.71	1.2	41.3	21.44	13.30	2.0
FAIRALL 49	15.4	22.77	15.61	1.5	27.7	22.01	12.85	1.3
FAIRALL 51	33.8	22.88	14.74	1.7	79.9	22.29	12.14	1.2
ESO 143-G09	39.9	22.42	13.89	1.8	61.4	22.35	11.66	1.3

TABLE 4—*Continued*

Name	Aperture B (arcsec)	3σ B (mag arcsec $^{-2}$)	B (mag)	(seeing B) (arcsec)	Aperture I (arcsec)	3σ I (mag arcsec $^{-2}$)	I (mag)	(seeing I) (arcsec)
FAIRALL 341	58.4	24.60	14.41	2.3	61.4	22.65	12.17	1.0
UGC 11630	29.2	22.10	14.60	1.1	78.3	21.91	11.79	1.0
PKS 2048–57	47.7	22.81	13.75	1.5	93.7	21.68	10.80	1.5
NGC 7213	69.1	22.25	11.75	1.5	190.5	21.84	8.86	1.3
MRK 915	24.6	22.57	15.21	1.1	53.8	22.76	12.41	1.0
UGC 12138	38.4	24.38	14.78	2.2	36.9	22.21	12.91	1.0
AKN 564	32.7	23.79	14.82	1.1	39.7	22.57	13.16	0.9
UGC 12348	30.7	22.34	15.78	1.2	38.4	20.32	13.25	1.2
NGC 7674	27.7	22.33	14.62	1.6	49.2	21.57	12.25	1.2
MRK 590	61.4	24.23	13.80	2.5	58.4	21.91	11.78	1.2
MRK 1058	35.7	23.94	15.52	2.1	37.7	22.19	13.21	1.2
NGC 1386	155.1	23.67	12.22	2.1	184.3	22.49	9.95	1.2
MCG +8-11-11	81.3	24.10	14.17	1.0	99.2	22.21	11.52	0.9
MRK 705	34.4	24.30	14.89	1.6	44.0	23.03	12.99	1.6
NGC 3281	178.2	24.45	12.82	1.1	184.3	22.36	10.44	1.2
UGC 6100	48.2	23.77	14.66	1.8	60.5	22.37	12.70	1.9
NGC 4941	190.5	24.18	12.30	1.0	192.0	22.17	10.16	1.1
UGC 10683B	27.5	23.31	16.13	1.3	—	—	—	—
ESO 103-G35	30.7	22.48	15.22	1.4	63.0	22.29	12.43	1.3
NGC 7212	30.7	22.60	15.60	1.5	27.7	20.14	13.34	1.3

Column 1 shows the galaxies names. Column 2 (6) presents the diameter of the ellipse major axis used to measure the galaxy flux in B (I); Column 3 (7) presents the surface brightness of the 3σ level above the background in B (I); Column 4 (8) presents the integrated B (I) magnitude; and Column 5 (9) presents the seeing during the observation.

TABLE 5
MAGNITUDES OF THE ADDITIONAL SAMPLE

Name	Aperture B (arcsec)	$3\sigma B$ (mag arcsec $^{-2}$)	B (mag)	(seeing B) (arcsec)	Aperture I (arcsec)	$3\sigma I$ (mag arcsec $^{-2}$)	I (mag)	(seeing I) (arcsec)
ESO 362-G8	63.0	24.34	13.36	1.4	70.7	22.67	11.45	1.0
NGC 2273	88.1	23.54	13.05	1.9	144.5	22.53	10.60	2.0
ESO 428-G14	89.1	24.32	13.47	1.2	107.5	21.84	10.83	1.0
MRK 78	24.8	23.83	15.56	2.2	33.0	23.41	13.51	1.4
NGC 2622	30.3	22.67	15.17	1.8	37.2	21.55	12.86	1.7
NGC 2639	77.1	23.23	12.92	1.7	114.2	22.46	10.55	2.2
UGC 5101	—	—	—	—	48.2	23.03	13.36	1.7
NGC 2992	—	—	—	—	115.2	22.25	10.96	1.1
NGC 3227	—	—	—	—	242.2	22.12	9.61	1.7
MRK 34	—	—	—	—	27.5	21.81	13.67	1.9
NGC 3362	—	—	—	—	59.2	22.42	12.32	1.8
MRK 423	—	—	—	—	34.4	21.09	13.18	2.1
NGC 5252	—	—	—	—	74.3	22.58	12.03	1.5
MRK 268	—	—	—	—	48.2	23.11	13.04	1.3
MRK 270	46.8	23.95	14.38	1.4	74.3	23.12	12.00	1.2
NGC 5273	114.2	23.86	12.70	1.3	151.4	22.88	10.52	1.7
IC 4329A	—	—	—	—	84.5	22.64	11.45	1.6
NGC 5929	55.0	22.74	14.02	1.3	41.3	20.54	12.23	1.2
NGC 7450	—	—	—	—	45.6	21.93	12.99	1.4
NGC 7672	—	—	—	—	48.6	22.52	13.00	1.6

Column 1 gives the galaxies names. Column 2 (6) presents the diameter of the ellipse major axis used to measure the galaxy flux in B (I); Column 3 (7) presents the surface brightness of the 3σ level above the background in B (I); Column 4 (8) presents the integrated B (I) magnitude; and Column 5 (9) presents the seeing during the observation.

TABLE 6
PA'S AND ELLIPTICITIES OF THE $60\mu\text{m}$ SAMPLE

Name	PA _{MA-I} (degrees)	e-I	PA _{MA-B} (degrees)	e-B
MRK 348	-45	0.061	-60	0.066
TOL 0109-38	61	0.555	61	0.507
MRK 1	70	0.361	67	0.347
MRK 359	8	0.167	-21	0.119
MRK 573	58	0.137	4	0.137
IRAS 01475-0740	-28	0.186	-35	0.161
ESO 153-G20	8	0.298	-50	0.465
MRK 1040	75	0.702	—	—
ESO 355-G25	-41	0.086	-29	0.076
UGC 2024	-30	0.373	-29	0.342
NGC 1068	-67	0.106	-5	0.196
MCG-02-08-039	12	0.434	17	0.451
UGC 2514	-40	0.428	-38	0.309
IRAS 03106-0254	-14	0.681	-17	0.585
IRAS 03125+0119	-32	0.439	-29	0.440
MRK 607	-42	0.616	-42	0.630
ESO 116-G18	—	—	-87	0.567
IRAS 04385-0828	44	0.517	44	0.493
IRAS 04502-0317	15	0.489	13	0.510
IRAS 04507+0358	46	0.192	52	0.310
ESO 33-G02	-88	0.086	-74	0.069
MCG-05-13-017	-41	0.193	-40	0.199
MRK 3	28	0.159	26	0.223
UGC 3478	44	0.623	43	0.518
MRK 6	-46	0.411	-48	0.379
FAIRALL 265	2	0.435	2	0.460
MRK 79	-47	0.186	69	0.393
MRK 10	-53	0.494	-44	0.513
UGC 4155	-40	0.231	-75	0.312
MRK 622	-35	0.098	-46	0.089
ESO 18-G09	-3	0.138	-22	0.140
MCG-01-24-012	42	0.414	38	0.527
MRK 1239	-25	0.188	-24	0.193
NGC 3393	41	0.131	48	0.128
NGC 3516	56	0.191	56	0.187
IRAS 11215-2806	-34	0.659	-34	0.649
MCG-05-27-013	-82	0.640	-82	0.663
MRK 176	59	0.609	59	0.612
NGC 3783	-46	0.074	-44	0.155
MRK 766	67	0.152	70	0.144
NGC 4388	-89	0.665	-88	0.722
NGC 4507	60	0.164	65	0.122
NGC 4593	-72	0.295	66	0.328
TOL 1238-364	72	0.104	81	0.078
NGC 4704	-61	0.083	-84	0.037
MCG-02-33-034	—	—	—	—
ESO 323-G32	-89	0.097	-70	0.091
MCG-04-31-030	58	0.531	58	0.529
IRAS 13059-2407	-59	0.669	-59	0.688
MCG-03-34-064	48	0.318	47	0.231
ESO 383-G18	88	0.546	88	0.552
MCG-6-30-15	-76	0.352	-74	0.359
NGC 5347	-60	0.211	-62	0.223
IRAS 14082+1347	-85	0.317	-83	0.305
NGC 5506	-89	0.755	-89	0.758
NGC 5548	-80	0.143	-87	0.198
IRAS 14317-3237	3	0.245	-1	0.249
IRAS 14434+2714	88	0.120	77	0.081
UGC 9826	-9	0.327	7	0.300
UGC 9944	-7	0.669	-7	0.676
IRAS 15480-0344	49	0.113	48	0.066
IRAS 16288+3929	-77	0.572	-77	0.568
IRAS 16382-0613	—	—	89	0.253
UGC 10889	43	0.580	45	0.598
MCG+03-45-003	-33	0.428	11	0.302
FAIRALL 49	-59	0.111	-28	0.186
FAIRALL 51	-22	0.447	2	0.576
ESO 143-G09	35	0.332	34	0.351

TABLE 6—*Continued*

Name	PA _{MA} -I (degrees)	e-I	PA _{MA} -B (degrees)	e-B
FAIRALL 341	-23	0.235	-26	0.228
UGC 11630	-81	0.530	-79	0.436
PKS 2048-57	-60	0.156	-62	0.167
NGC 7213	48	0.033	75	0.026
MRK 915	-7	0.507	-18	0.579
UGC 12138	-2	0.077	69	0.024
AKN 564	-73	0.198	-72	0.175
UGC 12348	-46	0.715	-46	0.708
NGC 7674	-26	0.266	76	0.228
MRK 590	-55	0.087	-73	0.068
MRK 1058	-68	0.418	-68	0.422
NGC 1386	25	0.628	25	0.638
MCG +8-11-11	54	0.190	1	0.514
MRK 705	77	0.226	80	0.225
NGC 3281	-39	0.589	-37	0.599
UGC 6100	17	0.336	21	0.360
NGC 4941	17	0.518	16	0.529
UGC 10683B	—	—	—	—
ESO 103-G35	39	0.597	40	0.610
NGC 7212	43	0.638	42	0.621

Column 1 gives the galaxy name; Columns 2 and 3 give the position angle (PA_{MA}) and the ellipticity of the major axis (e=1-b/a), and are also the values used to measure the I magnitudes; Columns 4 and 5 give the position angle and ellipticity of the ellipse used to measure the B magnitude, presented in Table 4.

TABLE 7
PA'S AND ELLIPTICITIES OF THE ADDITIONAL SAMPLE

Name	PA _{MA} -I (degrees)	e-I	PA _{MA} -B (degrees)	e-B
ESO 362-G8	-15	0.543	-16	0.537
NGC 2273	62	0.362	-87	0.356
ESO 428-G14	-44	0.343	-39	0.313
MRK 78	84	0.435	84	0.430
NGC 2622	52	0.332	52	0.329
NGC 2639	-43	0.398	-43	0.455
UGC 5101	79	0.417	—	—
NGC 2992	13	0.556	—	—
NGC 3227	-31	0.459	—	—
MRK 34	65	0.130	—	—
NGC 3362	0	0.062	—	—
MRK 423	—	—	—	—
NGC 5252	15	0.480	—	—
MRK 268	-67	0.415	—	—
MRK 270	-60	0.137	-61	0.156
NGC 5273	11	0.156	10	0.170
IC 4329A	44	0.464	—	—
NGC 5929	49	0.423	48	0.437
NGC 7450	25	0.321	—	—
NGC 7672	28	0.281	—	—

Column 1 gives the galaxy name; Columns 2 and 3 give the position angle (PA_{MA}) and the ellipticity of the major axis (e=1-b/a), and are also the values used to measure the I magnitudes; Columns 4 and 5 give the position angle and ellipticity of the ellipse used to measure the B magnitude, presented in Table 5.